

# Dynamics of Dissipative Nonlinear Systems: A Study via 2D CGLE by Contact Geometry

D.Y. Zhong<sup>1,2</sup> and G. Q. Wang<sup>2</sup>

<sup>1</sup>*State Key Laboratory of Hydroscience and Engineering, Tsinghua  
University, Beijing 10084, China*

<sup>2</sup>*Department of Hydraulic Engineering, Tsinghua University, Beijing 10084,  
China*

## Abstract

We develop a contact-geometric framework for dissipative nonlinear field theories by extending the least constraint theorem to complex fields and establishing a rigorous link with probability measures. The Complex Ginzburg-Landau Equation serves as a paradigmatic example, yielding a dissipative Contact Hamilton-Jacobi equation that governs the evolution of the action functional. Through canonical transformation and travelling-wave reduction, exact Jacobi elliptic solutions are obtained, revealing a continuous transition from periodic periodons to localised solitons. Probabilistic analysis identifies a universal switching line separating dynamical regimes and uncovers a first-order periodon-soliton phase transition with a hysteresis loop. The conserved contact potential emerges as the key geometric quantity governing pattern formation in dissipative media, analogous to energy in conservative systems.

**Keywords:** Contact Geometry; Complex Ginzburg-Landau Equation (CGLE); Dissipative Systems; Periodon-Soliton Transition; Probability Measure

# Contents

<b>1</b>	<b>Introduction</b>	<b>4</b>
<b>2</b>	<b>Contact Geometric Formulation for Complex Fields</b>	<b>6</b>
2.1	Least Constraint Theorem and Complex Field Extension . . . . .	6
2.1.1	Least Constraint Theorem for Real Vector Bundles . . . . .	6
2.1.2	Least Constraint Theorem for Complex Vector Bundles . . . . .	7
2.2	Contact Geometry of Probability Measure . . . . .	11
2.2.1	Evolution of Complex Structure . . . . .	11
2.2.2	Probability Measure of Vector Bundle . . . . .	15
<b>3</b>	<b>Geometric Dynamics of 2D CGLE</b>	<b>18</b>
3.1	2D CGLE and its Properties . . . . .	18
3.1.1	2D CGLE . . . . .	18
3.1.2	Nonlinear and Dissipative Nature of 2D CGLE . . . . .	19
3.2	Contact Dynamics of CGLE . . . . .	20
3.2.1	Contact Dynamical Equations of 2D CGLE . . . . .	20
3.2.2	Contact Hamilton–Jacobi Equation . . . . .	22
3.2.3	Conservation and Symmetry in 2D CGLE . . . . .	26
<b>4</b>	<b>Travelling-Wave Reduction and Analytical Solutions</b>	<b>29</b>
4.1	Travelling-Wave Reduction . . . . .	29
4.2	Solution of 2D CHJ Equation . . . . .	30
<b>5</b>	<b>Probabilistic View of State Transition in 2D CGLE</b>	<b>33</b>
5.1	Probability Density Function . . . . .	33
5.1.1	Probability Measure . . . . .	33
5.1.2	Normalisation . . . . .	35
5.2	Probabilistic Perspective of State Transitions . . . . .	37

5.2.1	Marginal Probability Density for $m$ . . . . .	37
5.2.2	Switching Line . . . . .	39
5.2.3	Hysteresis Loop of Periodon–Soliton Transitions . . . . .	43
<b>6</b>	<b>Concluding Remarks</b>	<b>47</b>
<b>A</b>	<b>Solution of Contact Hamilton-Jacobi Equation</b>	<b>48</b>

## List of Figures

1	Spatial visualisation of solutions to 2D CGLE. . . . .	34
---	--	----

## List of Theorems

2.1	Theorem (Least Constraint for Vector Bundles) . . . . .	6
2.2	Theorem (Least Constraint for Complex Vector Bundles) . . . . .	8
2.1	Lemma (Evolution of Complex Structure under Contact Flow) . . . . .	11
2.3	Theorem (Probability Measure of Vector Bundle) . . . . .	15
2.1	Remark . . . . .	17

## List of Tables

1	Travelling-wave parameters. . . . .	32
---	-------------------------------------	----

# 1 Introduction

Dissipative nonlinear equations describe dynamical behaviours prevalent in nonequilibrium systems, characterised by the ability of the system to maintain ordered spatiotemporal structures through the synergistic coupling of external driving, energy dissipation, and nonlinear interactions [1]. This behaviour is distinct from energy-conserving linear dynamics in conservative systems and from disordered processes dominated by pure dissipation [2, 3]. Such phenomena permeate multiscale physical scenarios from the macroscopic to the microscopic, including convective patterns in fluid media [4, 5], coherent light propagation in nonlinear optical systems [6], topological excitations in condensed matter systems [7], and pattern development in biological tissue.

Constructing a unified theoretical framework to analyse such dynamical mechanisms has become a key topic in nonlinear dynamics and mathematical physics. The Complex Ginzburg-Landau Equation (CGLE) [8], as a foundational model for describing nonequilibrium nonlinear systems, can precisely characterize the balance between driving forces (e.g., thermal buoyancy in convection, gain in optical systems) and dissipation (e.g., viscous dissipation, light absorption) [9], while capturing the phase transition from homogeneous steady states to ordered periodic patterns [10–16]. Its universality makes it a core tool connecting microscopic nonlinear dynamics to macroscopic observable dissipative nonlinear wave phenomena [17, 18].

Despite the CGLE’s essential role and broad applicability, research into its nonlinear wave dynamics remains an challenge [19–22]. Most existing methods rely on specific analytical techniques or system-specific numerical methods as discussed in [23, 24]. For instance, some studies tailor approximations to specific parameter regimes (e.g., weak nonlinearity or limited dissipation). In contrast, others focus on individual solution types (e.g., periodic waves or solitons) without linking them within a broader framework. This lack of a unified theoretical foundation not only limits the generalisability of conclusions from individual studies but also hinders systematic exploration of how different pattern types evolve into one another,

a crucial gap that emphasises the need for a more cohesive analytical framework [8].

For decades, one of the most significant ideas in the study of dynamics across a variety of disciplines has been the application of geometric methods to analyse complex spatiotemporal dynamics [25–27]. Many theoretical developments have shown that contact geometry provides a powerful framework for understanding dissipative structures in a unified manner [27–32]. In this paper, we develop a contact-geometric formulation of the CGLE, building on our previously reported study of the contact formulation of vector bundles [33], yielding a dissipative contact Hamilton-Jacobi-like equation that governs the evolution of dissipative structures. Our approach extends the classical Hamilton-Jacobi theory to dissipative systems by using contact geometry, which naturally accounts for energy dissipation. This formulation provides a framework for analysing the stability and dynamics of pattern-forming systems.

The main contributions of this work are as follows: (1) a contact-geometric formulation of dissipative nonlinear systems, (2) a dissipative contact Hamilton-Jacobi equation governing the evolution of the action functional, and (3) a probability measure within the contact-geometric framework, through which we analyse the first-order periodon–soliton phase-transition boundary and hysteresis loop in the contact-CGLE framework. This study not only enhances the theoretical foundation of pattern formation in dissipative systems but also provides a new analytical tool for studying complex spatiotemporal dynamics in various physical and biological systems.

The paper is organised as follows: Section 2 develops the contact-geometric formulation of a dissipative nonlinear system, extending the Least Constraint Theorem for vector bundles, deriving the contact dynamical equations, and establishing the probability density functional. Section 3 derives the dissipative contact Hamilton-Jacobi (CHJ) equation by generalising classical Hamilton-Jacobi theory to dissipative systems via contact geometry, introducing a canonical transformation to reduce 2D field dynamics to 1D problems, and formulating the equation. Section 4 discusses travelling-wave solutions of the CGLE by reducing the CHJ equation, obtaining solutions in Jacobi elliptic functions, analysing parameter conditions, and demonstrating the transition from periodic waves to solitons as the elliptic modulus

approaches unity, supported by detailed visualisations of the spatial distribution of field properties. Section 5 investigates the probabilistic properties of the 2D CGLE, deriving the probability density functional, defining the critical switching line, and exploring the periodon–soliton phase transition and hysteresis. Finally, Section 6 summarises the main contributions and the broader significance of the contact-geometric approach for nonlinear pattern formation in nonequilibrium systems.

## 2 Contact Geometric Formulation for Complex Fields

### 2.1 Least Constraint Theorem and Complex Field Extension

Contact geometry is a mathematical framework for addressing challenges in classical Hamiltonian mechanics applied to dissipative systems in which energy is not conserved [26, 27]. Unlike symplectic geometry, which applies to conservative systems [25], contact geometry employs a contact manifold defined by a contact 1-form  $\Theta$  that satisfies the non-degeneracy condition  $\Theta \wedge (d\Theta)^{\wedge n} \neq 0$  [26, 27]. This geometric structure naturally incorporates dissipation by allowing the system to evolve along extremal paths of a constraint function, rather than along conservative energy trajectories [33].

#### 2.1.1 Least Constraint Theorem for Real Vector Bundles

The core theoretical underpinning of contact geometry for vector bundles is its concluding theorem [33], which formalises the intrinsic contact geometric structure and the extremal evolution of stochastic dissipative systems. It reads:

**Theorem 2.1** (Least Constraint for Vector Bundles). *Let  $E \subset \mathbb{R}^n$  be an  $n$ -dimensional vector space and  $\mathbb{P}$  be the space of probability measures about  $E$ . The infinite-order stochastic jet bundle  $\pi_{E,0}^\infty : J^\infty(E, \mathbb{P}) \rightarrow E$  satisfies the following properties:*

1. *It admits a natural contact manifold  $(\mathcal{E}, \Theta)$  defined by the contact 1-form*

$$\Theta = dP - \varphi_i dy^i = \mathcal{H}dt - \varphi_i dy^i, \quad (2.1)$$

where  $\mathcal{E} = T^*E \times \mathbb{R}$ ;  $P \in \mathbb{P}$  is the probability measure;  $y \in E$ ,  $\varphi_i = B_i^{\mu_1 \dots \mu_\infty} P_{\mu_1 \dots \mu_\infty}$ , with  $P_{\mu_1 \dots \mu_\infty} = \partial_{\mu_1 \dots \mu_\infty} P$  and  $B_i^{\mu_1 \dots \mu_\infty}$  the coefficients, is the probability flux field, such that  $(y^i, \varphi_i, t) \in \mathcal{E}$ .  $\mathcal{H} = dP(\dot{y}) = \dot{y} \partial_y P$  is contact probability potential. The volume form  $\Theta \wedge (d\Theta)^{\wedge n}$  is non-degenerate, confirming a valid contact structure on  $J^\infty(E, \mathbb{P})$ .

2. There exists a unique vector field  $\mathfrak{X}(\mathcal{E}) = \{X_{\mathcal{H}} \mid X_{\mathcal{H}} \in \ker(d\Theta) \subset T\mathcal{E}\}$  such that:

$$\iota_{X_{\mathcal{H}}} \Theta = -\varepsilon, \quad \iota_{X_{\mathcal{H}}} d\Theta = 0, \quad (2.2)$$

where  $\varepsilon = \varphi_i \dot{y}^i - dP(\dot{y})$  constraint function. The Lie derivative  $L_{X_{\mathcal{H}}} \Theta = 0$  ensures the contact structure is preserved along the flow generated by  $\mathfrak{X}(\mathcal{E})$ .

3. The flow of  $\mathfrak{X}(\mathcal{E})$  corresponds to extremal paths of the action of  $\varepsilon$ , defined as

$$\mathcal{S} = \int \varepsilon dt = - \int \Theta. \quad (2.3)$$

This implies the system evolves to extremize  $\varepsilon$  while maximizing the variation of probability  $P$ . Moreover, there is a Hamilton-Jacobi-like equation for  $\mathcal{S}$ :

$$\frac{\partial \mathcal{S}}{\partial t} + \mathcal{H} \left[ y, \frac{\partial S}{\partial y}, t \right] = 0. \quad (2.4)$$

### 2.1.2 Least Constraint Theorem for Complex Vector Bundles

The above theorem is formulated for real vector bundles of  $E \subset \mathbb{R}^n$ , but the cases, for example, the systems of CGLE, describe complex amplitude field  $W \in \mathbb{C}^n$ . It is necessary to extend the contact geometric framework to complex vector fields. For the complex field  $W$  and its canonically conjugate field  $\Pi^* \in \mathbb{C}^n$  replacing the real local connection  $\varphi_i$ , the contact 1-form  $\Theta$  (Theorem 2.1, Property 1) is generalized to account for complex conjugacy. As a result, the extended contact manifold  $\mathcal{E}_{\mathbb{C}} = T^*E_{\mathbb{C}} \times \mathbb{R}$  with coordinates  $(W^j, \Pi_j^*, t)$ , and the contact 1-form:

$$\Theta_{\mathbb{C}} = \mathcal{H} dt - \Pi_j^* dW^j, \quad (2.5)$$

where  $\mathcal{H}$  is the complex contact potential. The non-degeneracy of  $\Theta_{\mathbb{C}} \wedge (d\Theta_{\mathbb{C}})^{\wedge n}$  is preserved, as  $dW^j$  and  $d\Pi_j^*$  are linearly independent complex differentials.

The real constraint function  $\varepsilon$  (Theorem 2.1, Property 2) is extended to complex fields by enforcing hermiticity. The complex constraint function is:

$$\varepsilon_{\mathbb{C}} = \Pi_j^* \dot{W}^j - \mathcal{H}. \quad (2.6)$$

Using the extended contact structure  $\Theta_{\mathbb{C}}$  and constraint  $\varepsilon_{\mathbb{C}}$ , the contact dynamical equations (Theorem 2.1, Property 3) are derived via the Poisson bracket generalised to complex functionals. The above extension can be summarised as the following theorem:

**Theorem 2.2** (Least Constraint for Complex Vector Bundles). *Let  $E_{\mathbb{C}}$  be an infinite-dimensional function space with values in  $\mathbb{C}^n$ , and let  $\mathbb{P}$  be the space of probability measures. The infinite-order stochastic jet bundle  $\pi_{E_{\mathbb{C}},0}^{\infty} : J^{\infty}(E_{\mathbb{C}}, \mathbb{P}) \rightarrow E_{\mathbb{C}}$  satisfies the following properties:*

(1) **Contact structure:** *There exists a natural contact manifold  $(\mathcal{E}_{\mathbb{C}}, \Theta_{\mathbb{C}})$  on  $J^{\infty}(E_{\mathbb{C}}, \mathbb{P})$ , defined by the contact 1-form*

$$\Theta_{\mathbb{C}} = \mathcal{H} dt - \Pi_j^*(\mathbf{r}, t) dW^j(\mathbf{r}, t), \quad (2.7)$$

where

- (a)  $\mathcal{E}_{\mathbb{C}} = T^* E_{\mathbb{C}} \times \mathbb{R}$  is extended complex phase space,
- (b)  $W^j(\mathbf{r}, t)$  is the complex field as a section of the complex vector bundle,
- (c)  $\Pi_j^*(\mathbf{r}, t) = B_j^{\mu_1 \dots \mu_{\infty}} P_{\mu_1 \dots \mu_{\infty}}$  is canonically conjugate field of  $W^j$ , and  $P_{\mu_1 \dots \mu_k} = \partial_{\mu_1 \dots \mu_k} P$  ( $k = 1, \dots, \infty$ ),
- (d)  $\mathcal{H} = \mathcal{H}[W, \Pi^*, t]$  is the complex contact potential.

The corresponding contact volume form is defined within the field-theoretic framework as:

$$\Omega_{\mathbb{C}} = \Theta_{\mathbb{C}} \wedge (d\Theta_{\mathbb{C}})^{\wedge n}, \quad (2.8)$$

where

$$n = \frac{1}{2} \text{rank} \left( d\Theta_{\mathbb{C}}|_{\ker \Theta_{\mathbb{C}}} \right) \quad (2.9)$$

is half the dimension of the transverse symplectic structure of the contact form.

(2) **Unique vector field:** There exists a unique vector field  $\mathfrak{X}(\mathcal{E}_{\mathbb{C}}) = \{X_{\mathcal{H}} \mid X_{\mathcal{H}} \in \ker(d\Theta_{\mathbb{C}}) \subset T\mathcal{E}_{\mathbb{C}}\}$  such that for

$$X_{\mathcal{H}} = \frac{\partial}{\partial t} + \dot{W}^i \frac{\partial}{\partial W^i} + \dot{\Pi}_i^* \frac{\partial}{\partial \Pi_i^*}, \quad (2.10)$$

it has that

$$\iota_{X_{\mathcal{H}}} \Theta_{\mathbb{C}} = -\varepsilon_{\mathbb{C}}, \quad \iota_{X_{\mathcal{H}}} d\Theta_{\mathbb{C}} = 0, \quad (2.11)$$

where  $\varepsilon_{\mathbb{C}} = \Pi_j^* \dot{W}^j - \mathcal{H}$  is a smooth complex constraint functional and satisfied that  $d\varepsilon_{\mathbb{C}} = 0$ . The Lie derivative  $L_{X_{\mathcal{H}}} \Theta_{\mathbb{C}} = 0$  guarantees that the contact structure is preserved along the flow generated by  $\mathfrak{X}(\mathcal{E}_{\mathbb{C}})$ .

(3) **Extremal paths and the contact Hamilton–Jacobi equation:** The flow of  $\mathfrak{X}(\mathcal{E}_{\mathbb{C}})$  corresponds to the extremal paths of the action functional of  $\varepsilon_{\mathbb{C}}$ , defined as

$$\mathcal{S} = \int \varepsilon_{\mathbb{C}} dt = - \int \Theta_{\mathbb{C}}. \quad (2.12)$$

This implies that the system evolves to extremize  $\varepsilon_{\mathbb{C}}$  while maximising the variation of the probability functional  $P$ . There exists a contact Hamilton–Jacobi-type equation:

$$\frac{\partial \mathcal{S}}{\partial t} + \mathcal{H} \left[ W, \frac{\partial \mathcal{S}}{\partial W}, t \right] = 0, \quad (2.13)$$

where  $\partial \mathcal{S} / \partial W = \Pi^*$ . Moreover,  $d\mathcal{S} = 0$  results in dynamical equations:

$$\begin{cases} \frac{\partial W^j}{\partial t} = \{W^j, \mathcal{H}\} = \frac{\partial \mathcal{H}}{\partial \Pi_j^*}, \\ \frac{\partial \Pi_j^*}{\partial t} = \{\Pi_j^*, \mathcal{H}\} = -\frac{\partial \mathcal{H}}{\partial W^j}, \\ \frac{\partial \varepsilon_{\mathbb{C}}}{\partial t} = -\{\varepsilon_{\mathbb{C}}, \mathcal{H}\}. \end{cases} \quad (2.14a)$$

$$(2.14b)$$

$$(2.14c)$$

For any two functionals  $F(W, \Pi^*)$  and  $G(W, \Pi^*)$ , the Poisson bracket in equation (2.14) is defined as:

$$\{F, G\} = \frac{\partial F}{\partial W^j} \frac{\partial G}{\partial \Pi_j^*} - \frac{\partial F}{\partial \Pi_j^*} \frac{\partial G}{\partial W^j}. \quad (2.15)$$

The complex field  $W$  and its canonically conjugate local connection  $\Pi^*$  form a pair of conjugate variables. Thus,

$$\{W^i, \Pi_j^*\} = \delta_j^i, \quad (2.16)$$

where  $\delta$  is the Dirac delta function. All other fundamental brackets vanish:

$$\{W^i, W^i\} = 0, \quad (2.17a)$$

$$\{\Pi_i^*, \Pi_i^*\} = 0. \quad (2.17b)$$

With the bracket defined above, the time evolution of any functional  $F(W, \Pi^*)$  is given by:

$$\frac{dF}{dt} = \{F, \mathcal{H}\} + \frac{\partial F}{\partial t}. \quad (2.18)$$

*Proof.* Details are the same as those of Theorem 2.1 as reported in [33], with the extension to complex vector bundles. The key steps are outlined as follows:

*Step 1: Complex Vector Bundle Setup:*

Define the complex vector space  $E_{\mathbb{C}}$  and its associated infinite-order stochastic jet bundle  $J^\infty(E_{\mathbb{C}}, \mathbb{P})$ , replacing the real vector space  $E$  in the original theorem with complex-valued fields  $W \in E_{\mathbb{C}} \subset \mathbb{C}^n$  and their canonically conjugate fields  $\Pi^* \in T^*E_{\mathbb{C}}$ .

*Step 2: Complex Contact Manifold Construction:* Generalize the real contact 1-form to the complex case

$$\Theta_{\mathbb{C}} = \mathcal{H}dt - \Pi_j^* dW^j, \quad (2.19)$$

Verify the non-degeneracy of the contact volume form

$$\Omega_{\mathbb{C}} = \Theta_{\mathbb{C}} \wedge (d\Theta_{\mathbb{C}})^{\wedge n} \quad (2.20)$$

by leveraging linear independence of  $dW^j$  and  $d\Pi_j^*$ .

*Step 3: Unique Vector Field Extension:* Extend the real vector field  $\mathfrak{X}(E)$  to  $\mathfrak{X}(E_{\mathbb{C}}) \subset \ker(d\Theta_{\mathbb{C}})$

$$\varepsilon_{\mathbb{C}} = \Pi_j^* \dot{W}^j - \mathcal{H}. \quad (2.21)$$

Confirm the conditions  $\iota_{X_{\mathcal{H}}} \Theta_{\mathbb{C}} = -\varepsilon_{\mathbb{C}}$  and  $\iota_{X_{\mathcal{H}}} d\Theta_{\mathbb{C}} = 0$ , and preserve the contact structure via  $L_{X_{\mathcal{H}}} \Theta_{\mathbb{C}} = 0$ .

*Step 4: Complex Poisson Bracket and Dynamical Equations:* Generalize the real Poisson bracket to complex functionals  $F(W, \Pi^*)$  and  $G(W, \Pi^*)$  as given in Eq. (2.15) derive the complex contact dynamical equations Eq. (2.14), and ensure consistency with the conjugate variable relation  $\{W^i, \Pi_j^*\} = \delta_j^i$ .

*Step 5: Extremal Paths and CHJ Equation:* Extend the real action functional  $\mathcal{S}$  to the complex case

$$\mathcal{S} = \int \varepsilon_{\mathbb{C}} dt = - \int \Theta_{\mathbb{C}}, \quad (2.22)$$

establish the relation  $\partial \mathcal{S} / \partial W^j = \Pi_j^*$ , and derive the contact Hamilton-Jacobi equation by extremizing  $\mathcal{S}$  while maximising the probability variation  $dP$ :

$$\frac{\partial \mathcal{S}}{\partial t} + \mathcal{H} \left[ W^j, \frac{\partial \mathcal{S}}{\partial W^j}, t \right] = 0. \quad (2.23)$$

□

## 2.2 Contact Geometry of Probability Measure

Within the contact-geometric approach developed in this study, the probability measure  $P[W]$  plays a fundamental role in characterising the statistical properties of dissipative structures. This subsection derives the explicit form of  $P[W]$  and provides its geometric interpretation.

### 2.2.1 Evolution of Complex Structure

**Lemma 2.1** (Evolution of Complex Structure under Contact Flow). *Let  $(\mathcal{E}, \Theta)$  be a complex contact manifold of complex dimension  $2n + 1$  with contact distribution  $\ker \Theta$  and induced symplectic form  $\omega = d\Theta|_{\ker \Theta}$ . Let  $X \in \mathfrak{X}(\mathcal{E})$  be the unique characteristic vector field satisfying*

*ing*

$$L_X \Theta = 0, \quad \iota_X \Theta = -\varepsilon, \quad \iota_X \omega = 0, \quad d\varepsilon(X) = 0.$$

Let  $J$  be an  $\omega$ -compatible complex structure on  $\ker \Theta$ . Define the intrinsic symplectic volume as follows. At each point  $p \in \mathcal{E}$ , choose a symplectic frame  $\{e_i, \tilde{e}_i\}_{i=1}^n \subset \ker \Theta$  satisfying

$$\tilde{e}_i = Je_i, \quad \omega(e_i, \tilde{e}_j) = \delta_{ij}, \quad \omega(e_i, e_j) = \omega(\tilde{e}_i, \tilde{e}_j) = 0. \quad (2.24)$$

Define

$$\mathcal{V}_{\text{int}} = \text{Re}[\omega^{\wedge n}(e_1, \tilde{e}_1, \dots, e_n, \tilde{e}_n)] \neq 0. \quad (2.25)$$

Then the Lie derivative of  $J$  along  $X$  must satisfy

$$L_X J = -\varepsilon J, \quad (2.26)$$

and consequently,

$$L_X \mathcal{V}_{\text{int}} = -n\varepsilon \mathcal{V}_{\text{int}}. \quad (2.27)$$

*Proof.* Step 1: Flow extension of symplectic frame.

Let  $\phi_t$  be the flow generated by the vector  $X$ . Fix  $p_0 \in \mathcal{E}$  and a symplectic frame  $\{e_i(0), \tilde{e}_i(0)\}$  at  $p_0$  satisfying the given conditions. Extend the frame along the integral curve  $p_t = \phi_t(p_0)$  by push-forward  $\phi_{t*}$  and transformation  $J(p_t)$ , respectively:

$$e_i(t) = \phi_{t*}e_i(0), \quad \tilde{e}_i(t) = J(p_t)e_i(t). \quad (2.28)$$

Define the pairing matrix  $A(t) = (A_{ij}(t))$  with  $A_{ij}(t) = \omega(e_i(t), \tilde{e}_j(t))$ . Since  $A(0) = I_n$ , we have  $\det A(0) = 1$ .

Step 2: Invariance under flow.

Noticing that  $(\phi_t^* J)(p_0)e_j(0) = \phi_{t*}^{-1}[J(p_t)(\phi_{t*}e_j(0))]$ , we had that

$$\phi_{t*}(\phi_t^* J)(p_0)e_j(0) = \phi_{t*}\phi_{t*}^{-1}[J(p_t)(\phi_{t*}e_j(0))] = J(p_t)(\phi_{t*}e_j(0)), \quad (2.29)$$

then using  $L_X \omega = 0$  (from  $L_X \Theta = 0$  and  $\omega = d\Theta|_{\ker \Theta}$ ), we express:

$$A_{ij}(t) = \omega(\phi_{t*}e_i(0), J(p_t)\phi_{t*}e_j(0)) = \omega(e_i(0), (\phi_t^* J)(p_0)e_j(0)). \quad (2.30)$$

Let  $J(t) = \phi_t^* J$  (pullback of  $J$ ) and  $F(t) = \det A(t)$ . Note that  $F(t) = \det A(t)$  and  $A(t)$  is the pairing matrix defined on the contact flow  $\phi_t$  (i.e., on the points of the integral curve  $p_t =$

$\phi_t(p_0)$ ), so  $F(t)$  is also a scalar quantity associated with  $\phi(t)$ . Then  $\mathcal{V}_{\text{int}} = \text{Re}[F(t)]$  (up to constant factor).

*Step 3: Evolution of complex structure.*

Differentiate  $A(t)$  at  $t = 0$ :

$$\dot{A}_{ij}(0) = \omega(e_i(0), \dot{J}(0)e_j(0)), \quad \dot{J}(0) = L_X J. \quad (2.31)$$

Consider the Hermitian metric  $h(U, V) = \omega(U, JV)$ . Compute:

$$L_X h(U, V) = (L_X \omega)(U, JV) + \omega(U, (L_X J)V) = \omega(U, (L_X J)V), \quad (2.32)$$

since  $L_X \omega = 0$ . For  $h$  to remain Hermitian,  $L_X h = \lambda h$  for some  $\lambda$ , implying  $L_X J = \lambda J$ .

To determine  $\lambda$ , use the contact condition  $\iota_X \Theta = -\varepsilon$  and  $X(\varepsilon) = 0$  (so  $\varepsilon$  is constant). The contact form  $\Theta$  induces  $\omega = d\Theta|_{\ker \Theta}$ , and the flow of  $X$  scales  $\Theta$  by  $-\varepsilon$  (since  $\iota_X \Theta = -\varepsilon$ ). As  $J$  is  $\omega$ -compatible, its evolution must match this scaling:

$$L_X J = -\varepsilon J. \quad (2.33)$$

*Step 4: Volume evolution.*

To establish the key identity linking the time derivative of the pullback of the complex structure  $J$  to the pullback of its Lie derivative along the characteristic vector field  $X$ , we proceed as follows:

Let  $\phi_t : E \rightarrow E$  denote the one-parameter diffeomorphism group (flow) generated by  $X$ , satisfying the group operation  $\phi_{t+s} = \phi_t \circ \phi_s$  for all  $t, s \in \mathbb{R}$ . By the composition law of pullback operations for diffeomorphisms, we have  $(\phi_t \circ \phi_s)^* J = \phi_s^*(\phi_t^* J)$ , which simplifies to  $\phi_{t+s}^* J = \phi_s^*(\phi_t^* J)$  due to the group structure.

Next, we define the time derivative of the pullback tensor field  $\phi_t^* J$ . For a fixed  $t$ , the derivative with respect to  $t$  is given by the limit of the difference quotient as  $s \rightarrow 0$ , i.e.,

$$\frac{d}{dt}(\phi_t^* J) = \frac{d}{ds} \bigg|_{s=0} \phi_{t+s}^* J. \quad (2.34)$$

This expression captures the instantaneous rate of change of  $\phi_t^* J$  along the flow generated by  $X$ .

Substituting the group property  $\phi_{t+s}^* J = \phi_s^*(\phi_t^* J)$  into the derivative definition, we rewrite the right-hand side as

$$\frac{d}{dt}(\phi_t^* J) = \frac{d}{ds} \bigg|_{s=0} \phi_s^*(\phi_t^* J). \quad (2.35)$$

Recall the flow-based definition of the Lie derivative: for any tensor field  $T$ , the Lie derivative along  $X$  is  $\mathcal{L}_X T = \frac{d}{ds} \bigg|_{s=0} \phi_s^* T$ . Identifying  $T = \phi_t^* J$  in this definition, the right-hand side of the above equation is exactly  $\mathcal{L}_X(\phi_t^* J)$ , leading to

$$\frac{d}{dt}(\phi_t^* J) = \mathcal{L}_X(\phi_t^* J). \quad (2.36)$$

We now invoke the commutativity between pullback and Lie derivative for the flow  $\phi_t$  generated by  $X$ . For any diffeomorphism  $\phi_s$  in the group and any tensor field  $T$ , the pullback preserves the Lie derivative, i.e.,  $\phi_s^*(\mathcal{L}_X T) = \mathcal{L}_X(\phi_s^* T)$ . Setting  $s = t$  and  $T = J$ , this commutativity yields  $\mathcal{L}_X(\phi_t^* J) = \phi_t^*(\mathcal{L}_X J)$ . Combining the two results above, we arrive at the desired identity:

$$\frac{d}{dt}(\phi_t^* J) = \phi_t^*(\mathcal{L}_X J). \quad (2.37)$$

The flow  $\phi_t$  of  $X$  scales the complex structure exponentially:

$$\phi_t^* J = e^{-\int \varepsilon dt} J. \quad (2.38)$$

Recall the definition  $A_{ij}(t) = \omega(e_i(t), J e_j(t))$  with the frame  $e_i(t) = \phi_{t*} e_i(0)$ . Using the invariance  $L_X \omega = 0$  (which follows from  $L_X \Theta = 0$  and  $\omega = d\Theta|_{\ker \Theta}$ ) we obtain

$$\begin{aligned} A_{ij}(t) &= \omega(\phi_{t*} e_i(0), J(p_t) \phi_{t*} e_j(0)) \\ &= \omega(e_i(0), (\phi_t^* J)(p_0) e_j(0)) \\ &= e^{-\varepsilon t} \omega(e_i(0), J(p_0) e_j(0)). \end{aligned} \quad (2.39)$$

At  $t = 0$  the frame was chosen so that  $\omega(e_i(0), J e_j(0)) = \delta_{ij}$ ; therefore

$$A(t) = e^{-\int \varepsilon dt} I_n. \quad (2.40)$$

Consequently,

$$F(t) = \det A(t) = e^{-n \int \varepsilon dt}, \quad (2.41)$$

and its derivative is

$$\dot{F}(t) = -n\varepsilon e^{-n\int \varepsilon dt} = -n\varepsilon F(t). \quad (2.42)$$

Evaluating at  $t = 0$  gives  $\dot{F}(0) = -n\varepsilon$ , which is consistent with the computation via Jacobi's formula. Since (2.42) holds for every  $t$ , the Lie derivative of  $F$  satisfies

$$L_X F = -n\varepsilon F. \quad (2.43)$$

Finally, the intrinsic symplectic volume is defined as  $\mathcal{V}_{\text{int}} = \text{Re}[F]$  (up to a constant factor). Because  $\varepsilon$  is real, taking the real part commutes with the Lie derivative, yielding

$$L_X \mathcal{V}_{\text{int}} = \text{Re}[L_X F] = \text{Re}[-n\varepsilon F] = -n\varepsilon \text{Re}[F] = -n\varepsilon \mathcal{V}_{\text{int}}. \quad (2.44)$$

*Step 5: Normalisation independence.*

If  $\omega(e_i, \tilde{e}_j) = c\delta_{ij}$ , then  $F(0) = c^n$  and  $\dot{F}(0) = -n\varepsilon c^n$ , so the evolution equation holds for any frame normalization.  $\square$

### 2.2.2 Probability Measure of Vector Bundle

Based on the lemma given above, we can establish the following theorem:

**Theorem 2.3** (Probability Measure of Vector Bundle). *In the setting of Theorem 2.2, consider the contact manifold  $(\mathcal{E}_{\mathbb{C}}, \Theta_{\mathbb{C}})$ , the contact volume form  $\Omega_{\mathbb{C}} = \Theta_{\mathbb{C}} \wedge (d\Theta_{\mathbb{C}})^{\wedge n}$ , the unique vector field  $X_{\mathcal{H}}$ , and the action functional  $\mathcal{S} = -\int \Theta_{\mathbb{C}}$ . Let  $\pi : \mathcal{E}_{\mathbb{C}} \rightarrow E_{\mathbb{C}}$  be the projection  $\pi(t, W, \Pi^*) = W$ . Then, there exists a probability density functional on space  $E_{\mathbb{C}}$  of the form*

$$\mathcal{P}[W] = \frac{1}{\mathcal{Z}} \exp(n\mathcal{S}[W]), \quad \mathcal{Z} = \int_{E_{\mathbb{C}}} \exp(n\mathcal{S}[W]) \mathcal{D}W, \quad (2.45)$$

where  $\mathcal{S}[W] = -\int \Theta_{\mathbb{C}}$  is the action functional defined in Theorem 2.2, and  $\mathcal{D}W$  denotes the formal volume element on  $E_{\mathbb{C}}$ .

*Proof.* We proceed through the following geometrically motivated steps.

*Step 1: Finite-dimensional approximation of the contact structure.*

Consider a complex contact manifolds  $(\mathcal{E}_{\mathbb{C}}, \Theta_{\mathbb{C}})$  with  $\dim_{\mathbb{C}} \mathcal{E}_{\mathbb{C}} = 2n + 1$ , where

$$n = \frac{1}{2} \operatorname{rank}_{\mathbb{C}} \left( d\Theta_{\mathbb{C}}|_{\operatorname{Ker} \Theta_{\mathbb{C}}} \right). \quad (2.46)$$

Each manifold satisfies the non-degeneracy condition

$$\Theta_{\mathbb{C}} \wedge d\Theta_{\mathbb{C}}^{\wedge n} \neq 0, \quad (2.47)$$

and carries the induced symplectic form on the contact distribution:

$$\omega_{\mathbb{C}} = d\Theta_{\mathbb{C}}|_{\operatorname{Ker} \Theta_{\mathbb{C}}}. \quad (2.48)$$

By Theorem 2.2, there exists a unique vector field  $X_{\mathcal{H}}$  satisfying

$$\iota_{X_{\mathcal{H}}} \Theta_{\mathbb{C}} = -\varepsilon_{\mathbb{C}}, \quad \iota_{X_{\mathcal{H}}} \omega_{\mathbb{C}} = 0, \quad (2.49)$$

where  $\varepsilon_{\mathbb{C}} = \partial_t \mathcal{S}$  and  $\mathcal{S} = -\int \Theta_{\mathbb{C}}$  is the action functional. Let  $\pi : \mathcal{E}_{\mathbb{C}} \rightarrow E_{\mathbb{C}}$  denote the canonical projection.

*Step 2: Intrinsic symplectic volume evolution.*

On contact distribution  $\operatorname{Ker} \Theta_{\mathbb{C}}$ , choose a symplectic frame  $\{e_1, Je_1, \dots, e_n, Je_n\}$  as in the Lemma, and define the intrinsic symplectic volume

$$\mathcal{V}_{\text{int}} = \operatorname{Re} \left[ (\omega_{\mathbb{C}})^{\wedge n} (e_1, Je_1, \dots, e_n, Je_n) \right] \neq 0. \quad (2.50)$$

According to Lemma 2.1, the Lie derivative of  $\mathcal{V}_{\text{int}}$  along  $X_{\mathcal{H}}$  satisfies

$$\mathcal{L}_{X_{\mathcal{H}}} \mathcal{V}_{\text{int}} = -n \varepsilon_{\mathbb{C}} \mathcal{V}_{\text{int}}. \quad (2.51)$$

*Step 3: Construction of an invariant measure along the characteristic flow.*

From the evolution equation (2.51), we obtain

$$\begin{aligned} \mathcal{V}_{\text{int}}(t) &= \mathcal{V}_{\text{int}}(0) \exp \left( -n \int_0^t \varepsilon_{\mathbb{C}}(s) ds \right) \\ &= \mathcal{V}_{\text{int}}(0) \exp \left( -n(\mathcal{S}(t) - \mathcal{S}(0)) \right). \end{aligned} \quad (2.52)$$

Consequently,

$$\mathcal{I} = \mathcal{V}_{\text{int}}(t) \exp(n\mathcal{S}(t)) = \mathcal{V}_{\text{int}}(0) \exp(n\mathcal{S}(0)). \quad (2.53)$$

This shows that the quantity  $\mathcal{I}$  is constant along the characteristic flow, i.e.,  $\mathcal{L}_{X_{\mathcal{H}}}\mathcal{I} = 0$ .

Therefore, we can define the measure  $\mu$  as

$$\mu dt = \exp(n\mathcal{S}(t, W)) \mathcal{V}_{\text{int}}(t) dt \wedge d^{\wedge n}W = \mathcal{I} dt \wedge d^{\wedge n}W. \quad (2.54)$$

*Step 4: Pushforward to the configuration space and emergence of the probability density.*

We now push forward the measure  $\mu$  to the configuration space  $E_{\mathbb{C}}$ . The projection  $\pi : \mathcal{E}_{\mathbb{C}} \rightarrow E_{\mathbb{C}}$  sends  $(W, \Pi^*)$  to  $W$ . For a measurable set  $A$  in  $E_{\mathbb{C}}$ , we have

$$((\pi)_*\mu)(A) = \int_{\pi^{-1}(A)} \mu = \int_A \mathcal{I} d^nW. \quad (2.55)$$

Thus, we define a probability measure on  $E_{\mathbb{C}}$  by

$$dP(W) = \frac{1}{\mathcal{Z}} \mathcal{I} d^nW, \quad \mathcal{Z} = \int_{E_{\mathbb{C}}} \mathcal{I} d^nW. \quad (2.56)$$

Here we assume  $0 < \mathcal{Z} < \infty$ , i.e., the measure is normalizable.  $\square$

**Remark 2.1.** *This theorem reveals two fundamental geometric interpretations of the probability density functional  $\mathcal{P}[W]$  in the contact-geometric framework:*

1. *Probability as Information Compression via Projection:* The probability measure  $P[W]$  is essentially the result of information compression induced by the canonical projection  $\pi : \mathcal{E}_{\mathbb{C}} \rightarrow E_{\mathbb{C}}$ , which maps the high-dimensional contact manifold  $E_{\mathbb{C}}$  with coordinates  $(t, W, \Pi^*)$  to the low-dimensional configuration space of the complex field  $W$ . The invariant

$$\mathcal{I} = \mathcal{V}_{\text{int}}(t) \exp(n\mathcal{S}(t))$$

serves as the core carrier of the geometric and dynamical information from the high-dimensional contact structure; its conservation ensures that the compressed information remains stable along the contact flow, without loss of key geometric constraints during the projection process.

2. *Information Encoding into the Action Functional: The compressed geometric and statistical information is ultimately encapsulated in the action functional*

$$\mathcal{S} = - \int \Theta_{\mathbb{C}}$$

*The exponential form of the probability density functional  $\mathcal{P}[W] \propto \exp(n\mathcal{S}[W])$  directly reflects that the statistical weight of any field configuration  $W$  is determined by the action  $\mathcal{S}$ , which aggregates the compressed information from the high-dimensional contact manifold. This establishes a direct link between the geometric invariant  $\mathcal{I}$ , the action functional  $\mathcal{S}$ , and the statistical properties of dissipative structures described by  $\mathcal{P}[W]$ .*

### 3 Geometric Dynamics of 2D CGLE

#### 3.1 2D CGLE and its Properties

##### 3.1.1 2D CGLE

In this paper, we study the 2D CGLE for studying dispersive waves given in [5, 34, 35] as follows

$$\frac{\partial W}{\partial t} = \mu W - |W|^2 W + \left( \partial_x - \frac{i}{2} \partial_y^2 \right)^2 W, \quad (3.1)$$

where we use  $\partial_x$  and  $\partial_y$  stand for, respectively,  $\frac{\partial}{\partial x}$  and  $\frac{\partial}{\partial y}$ .

The two-dimensional Complex Ginzburg-Landau Equation (2D CGLE) in Eq. (3.1) is a fundamental model for investigating the evolution of dispersive waves.  $W = W(x, y, t)$  denotes the complex amplitude of dispersive waves, a complex-valued function dependent on the two-dimensional spatial coordinates  $x, y$  and the time variable  $t$ . The modulus  $|W|$  quantifies the amplitude magnitude of the wave, while the argument of  $W$  characterises the phase distribution of the wave; thus,  $W$  is the core dependent variable that describes both the amplitude and phase evolution of dispersive waves.

The composite dispersive operator  $\left( \partial_x - \frac{i}{2} \partial_y^2 \right)^2$  is the core of the dispersive wave model,

which can be expanded as:

$$\left(\partial_x - \frac{i}{2}\partial_y^2\right)^2 = \partial_x^2 - i\partial_x\partial_y^2 - \frac{1}{4}\partial_y^4, \quad (3.2)$$

This operator encapsulates three key dispersive effects: (1)  $\partial_x^2$  represents second-order dispersion along the  $x$ -direction (wave velocity dependence on frequency); (2)  $-i\partial_x\partial_y^2$  denotes mixed dispersion between the  $x$ - and  $y$ -directions (dispersion coupling across orthogonal spatial directions); (3)  $-\frac{1}{4}\partial_y^4$  corresponds to fourth-order dispersion along the  $y$ -direction, a high-order correction for strong dispersion regimes.

### 3.1.2 Nonlinear and Dissipative Nature of 2D CGLE

The right-hand side of Eq. (3.1) consists of three terms, corresponding to linear effects, nonlinear effects, and dispersive effects, respectively.  $\mu$  is a real constant defined as the linear gain/loss parameter, which governs the linear evolution tendency of the wave and determines system stability;  $-|W|^2W$  is a cubic nonlinear saturation term, where  $|W|^2 = W^*W$  ( $W^*$  is the complex conjugate of  $W$ , making  $|W|^2$  a real-valued function). This term describes wave self-interaction, and the negative sign embodies the saturation effect: as  $|W|$  increases, this term suppresses unbounded amplitude growth, enabling a balance between dispersive and nonlinear effects. This balance is the core mechanism for the formation of stable wave structures (e.g., solitons, periodic patterns, localised wave packets) in dispersive wave systems.

To understand the essential nature of the CGLE, we define a 2D differential operator  $\mathcal{L}$  as:

$$\mathcal{L} = \partial_x - \frac{i}{2}\partial_y^2. \quad (3.3)$$

For complex functions  $f, g \in \mathbb{C}^\infty$  decaying at infinity, the adjoint  $\mathcal{L}^\dagger$  is defined by:

$$\langle f, \mathcal{L}g \rangle \equiv \iint f^*(\mathcal{L}g) dx dy = \iint (\mathcal{L}^\dagger f)^* g dx dy. \quad (3.4)$$

Through integration by parts and by vanishing conditions of boundary terms, we had that

$$\langle f, \mathcal{L}g \rangle = \iint \left[ (\partial_x f)^* - \left(-\frac{i}{2}\right)^* (\partial_y^2 f)^* \right] g dx dy. \quad (3.5)$$

Since  $\left(-\frac{i}{2}\right)^* = \frac{i}{2}$ , this leads to define that:

$$\mathcal{L}^\dagger = -\partial_x + \frac{i}{2}\partial_y^2, \quad (3.6)$$

confirming the skew-adjoint property  $\mathcal{L}^\dagger = -\mathcal{L}$ .

The skew-adjoint property  $\mathcal{L}^\dagger = -\mathcal{L}$  plays a pivotal role in the dynamics of the CGLE and the study of dispersive waves. First, it imposes a rigid constraint on the spectrum of  $\mathcal{L}$ , ensuring all eigenvalues are purely imaginary—this directly translates to the oscillatory and nondissipative propagation of dispersive wave modes, as the linear evolution generated by  $\mathcal{L}$  (and its square  $\mathcal{L}^2$  in the CGLE) avoids exponential growth or decay inherent to dissipative/amplifying systems. Second, the skew-adjointness guarantees that  $\mathcal{L}^2 = -\mathcal{L}^\dagger\mathcal{L}$  is a self-adjoint operator, whose real spectrum underpins the well-posedness of the CGLE's linearization and simplifies the decomposition of dispersive wave modes. Third, this property preserves the conservative nature of the dispersive term in the equation, distinguishing it from the nonlinear ( $|W|^2W$ ) and gain/loss ( $\mu W$ ) terms, thereby providing a mathematical foundation for analyzing the stability, periodicity, and propagation characteristics of dispersive waves described by the CGLE.

## 3.2 Contact Dynamics of CGLE

### 3.2.1 Contact Dynamical Equations of 2D CGLE

In the above equations,  $\mathcal{H}$  can be determined by

$$\varepsilon_C = \Pi^* \dot{W} - \mathcal{H}, \quad \dot{W} = \partial \mathcal{H} / \partial \Pi^* \implies \varepsilon_C = \Pi^* \frac{\partial \mathcal{H}}{\partial \Pi^*} - \mathcal{H}, \quad (3.7)$$

with the solution [33]:

$$\mathcal{H}[W, \Pi^*, t] = \mathcal{H}_{\text{par}}[W, \Pi^*, t] + \mathcal{H}_{\text{hom}}[W, \Pi^*, t], \quad (3.8)$$

of which  $\mathcal{H}_{\text{hom}}[W, \lambda \Pi^*, t] = \lambda \mathcal{H}_{\text{hom}}[W, \Pi^*, t]$  for  $\lambda \neq 0$ .

In the contact-geometric framework, the component  $\mathcal{H}_{\text{par}}$  imposes constraints not only on the geometry of the configuration space. With  $\mathcal{H}_{\text{par}}$  explicitly incorporated into the

dynamical equations, they can, in principle, yield direct solutions tailored to the prescribed configuration, boundary, and initial conditions. However, retaining  $\mathcal{H}_{\text{par}}$  in the equations substantially complicates their solution.

To simplify the analysis while preserving the non-degeneracy of the contact structure, we impose the constraint function to be a non-zero constant  $C$ , corresponding to  $\mathcal{H}_{\text{par}} = C$ . This yields the constraint  $\varepsilon_{\mathbb{C}} = -C \neq 0$ , ensuring the contact form remains non-degenerate. However, this choice corresponds to a trivial particular solution—a constant solution that does not contribute to the system’s essential dynamics. Since constant terms do not affect the Poisson bracket structure, the equations of motion are entirely generated by the homogeneous part  $\mathcal{H}_{\text{hom}}$ .

In line with standard practice in dynamical system analysis, we therefore derive the general solutions using the homogeneous contact potential  $\mathcal{H}_{\text{hom}}$  and subsequently impose the relevant constraints. This approach yields the same dynamical equations as setting  $\mathcal{H}_{\text{par}} = 0$  but avoids the theoretical issue of contact form degeneracy, allowing us to focus on the non-trivial dynamics of the system.

Thus:

$$\mathcal{H} = -(\mathcal{L}W)(\mathcal{L}\Pi^*) + \mu W\Pi^* - |W|^2 W\Pi^*. \quad (3.9)$$

In fact, we had that

$$\begin{aligned} \mathcal{H} &= \Pi^* \mathcal{L}^2 W + \mu W\Pi^* - |W|^2 W\Pi^* \\ &= \Pi^* [\mathcal{L}^2 W + \mu W - |W|^2 W] \\ &= \Pi^* \dot{W}. \end{aligned} \quad (3.10)$$

Clearly,  $\mathcal{H}(W, \lambda\Pi^*) = \lambda\mathcal{H}(W, \Pi^*)$ , and thus it is a homogeneous solution as required. Moreover, The contact potential  $\mathcal{H} = \Pi^* \dot{W}$  inherently carries a power-like physical meaning:  $\Pi^*$ , as the probability gradient, acts as a “driving force” that quantifies the most probable evolutionary direction of the system’s state, while  $\dot{W}$  describes the time rate of change of the complex field’s amplitude and phase, reflecting the intensity of the system’s dynamic evolution. Their product directly corresponds to the power of energy exchange between the system and its environment: positive values indicate energy input to drive the formation of

ordered structures such as solitons, while negative values represent energy dissipation that maintains the dynamic balance of the system. This aligns with the core characteristic of dissipative systems relying on continuous energy exchange to sustain spatiotemporal order. Unlike the energy conservation in conservative systems, this power-like nature of the contact potential further explains why it becomes the key geometric quantity governing pattern formation in dissipative media, linking the statistical information of probability gradients to the dynamic evolution of the field in a unified contact-geometric framework.

Using the Poisson bracket definition and functional derivatives:

$$\frac{\partial W}{\partial t} = \{W, \mathcal{H}\} = \frac{\partial W}{\partial W} \frac{\partial \mathcal{H}}{\partial \Pi^*} - \frac{\partial W}{\partial \Pi^*} \frac{\partial \mathcal{H}}{\partial W} = \frac{\partial \mathcal{H}}{\partial \Pi^*(\mathbf{r})}. \quad (3.11)$$

We compute the functional derivatives of the contact potential:

$$\begin{aligned} \dot{W} &= \frac{\partial \mathcal{H}}{\partial \Pi^*} = \frac{\partial}{\partial \Pi^*} \left[ -(\mathcal{L}W)(\mathcal{L}\Pi^*) + \mu W\Pi^* - |W|^2 W\Pi^* \right] \\ &= \mathcal{L}^2 W + \mu W - |W|^2 W, \end{aligned} \quad (3.12)$$

which is exactly the CGLE. Similarly

$$\begin{aligned} \dot{\Pi}^* &= -\frac{\partial \mathcal{H}}{\partial W} = -\frac{\partial}{\partial W} \left[ -(\mathcal{L}W)(\mathcal{L}\Pi^*) + \mu W\Pi^* - |W|^2 W\Pi^* \right] \\ &= -\mathcal{L}^2 \Pi^* - \mu \Pi^* + 2|W|^2 \Pi^*. \end{aligned} \quad (3.13)$$

### 3.2.2 Contact Hamilton–Jacobi Equation

The Hamilton–Jacobi (HJ) equation is a foundational tool in dynamical systems that relates the action functional to the Hamiltonian, thereby enabling the solution of complex dynamics via action extremisation. For dissipative systems described by contact geometry (Section 2), the classical HJ equation generalises to the contact HJ equation (CHJ), which retains the contact manifold's geometric structure while accounting for dissipation.

For classical Hamiltonian systems, the HJ equation is derived from the action functional  $S[q, t]$  and Hamiltonian  $H(q, p, t)$ , where  $q$  denotes generalised coordinates and  $p = \partial S / \partial q$  as canonical momentum. It takes the form:

$$\frac{\partial S}{\partial t} + H \left( q, \frac{\partial S}{\partial q}, t \right) = 0.$$

This equation describes the evolution of the action functional that extremizes the system's dynamics.

In the contact geometric framework of CGLE, the contact potential  $\mathcal{H}[W, \Pi^*, t]$  (Eq. (3.9)) replaces the classical Hamiltonian. The action functional  $S[W, t]$  is defined such that the canonical conjugate field  $\Pi^*(\mathbf{r}, t)$  to complex field  $W$  is the functional derivative of the action:

$$\Pi^*(\mathbf{r}, t) = \frac{\partial S[W, t]}{\partial W(\mathbf{r}, t)}. \quad (3.14)$$

Substituting this relation into the contact dynamical equation for the action functional (2.18), with no explicit time dependence of  $\mathcal{H}$ , we get the CHJ equation for the 2D CGLE:

$$\frac{\partial S}{\partial t} + \mathcal{H} \left[ W, \frac{\partial S}{\partial W}, t \right] = 0. \quad (3.15)$$

This is the core equation of this study, which governs the evolution of the action functional  $S[W, t]$  in the contact geometric framework.

The direct solution of Eq. (3.15) is challenging due to the complex-valued field  $W(\mathbf{r}, t) \in \mathbb{C}$  and 2D functional space. To simplify the equation and enable analytical solutions, we introduce a canonical transformation that maps the complex field  $W$  and its conjugate field  $\Pi^*$  to a real-valued field and its corresponding conjugate field, preserving the canonical Poisson bracket structure, which is critical for consistency with contact dynamics.

We define a canonical field transformation that converts the complex scalar field  $W(\mathbf{r}, t) \in \mathbb{C}$  and its conjugate connection  $\Pi^*(\mathbf{r}, t) \in \mathbb{C}$  to a real field  $\Phi(y, t) \in \mathbb{R}$  and its canonical counterpart  $\Pi_\Phi(y, t) \in \mathbb{R}$ . The transformation is performed at a fixed field intensity  $J$ , treated as a time-independent external parameter once the system reaches a statistical steady state such that  $\partial J / \partial t = 0$ .

We define a type-2 generating functional  $F_2[W, \Pi_\Phi, t]$  that depends on the original complex field  $W(y, t)$  and the new real conjugate field  $\Pi_\Phi(y, t)$ :

$$F_2[W, \Pi_\Phi, t] = \sqrt{\frac{2\pi}{J}} \exp(-i(k_x x + \theta(y, t)) + \phi(y)) W(\mathbf{r}, t) \Pi_\Phi(y, t), \quad (3.16)$$

where  $k_x \in \mathbb{R}$  is the fixed wavenumber in the  $x$ -direction;  $\theta(y, t) \in \mathbb{R}$  is a  $y$ -dependent

phase ensuring consistency between complex and real descriptions,  $\phi(y) \in \mathbb{R}$ ;  $J > 0$  is the conserved total intensity  $J = \iint_{\mathbb{R}^2} |W(\mathbf{r}, t)|^2 d^2\mathbf{r}$ .

The functional derivatives of  $F_2$  determine the canonical transformation:

$$\left\{ \begin{array}{l} \Pi^*(\mathbf{r}, t) = \frac{\partial F_2}{\partial W(\mathbf{r}, t)} = \sqrt{\frac{2\pi}{J}} \exp(-i(k_x x + \theta(y, t) + \phi(y))) \Pi_\Phi(y, t), \end{array} \right. \quad (3.17a)$$

$$\left\{ \begin{array}{l} \Phi(y, t) = \frac{\partial F_2}{\partial \Pi_\Phi(y, t)} = \sqrt{\frac{2\pi}{J}} \exp(-i(k_x x + \theta(y, t) + \phi(y))) W(\mathbf{r}, t). \end{array} \right. \quad (3.17b)$$

Solving these relations explicitly gives the direct transformation:

$$\left\{ \begin{array}{l} W(\mathbf{r}, t) = \sqrt{\frac{J}{2\pi}} \exp(i(k_x x + \theta(y, t) + \phi(y))) \Phi(y, t), \end{array} \right. \quad (3.18a)$$

$$\left\{ \begin{array}{l} \Pi^*(\mathbf{r}, t) = \sqrt{\frac{2\pi}{J}} \exp(-i(k_x x + \theta(y, t) + \phi(y))) \Pi_\Phi(y, t), \end{array} \right. \quad (3.18b)$$

with the normalization condition  $\int_{-\infty}^{\infty} \Phi^2(y, t) dy = 1$  ensuring conservation of total intensity.

To confirm the transformation is canonical, we compute the fundamental Poisson bracket  $\{\Phi(y), \Pi_\Phi(y')\}$ . Using the standard chain rule for functional brackets, we have

$$\{\Phi(y), \Pi_\Phi(y')\} = \frac{\partial \Phi(y)}{\partial W(\tilde{\mathbf{r}})} \frac{\partial \Pi_\Phi(y')}{\partial \Pi^*(\tilde{\mathbf{r}})} - \frac{\partial \Phi(y)}{\partial \Pi^*(\tilde{\mathbf{r}})} \frac{\partial \Pi_\Phi(y')}{\partial W(\tilde{\mathbf{r}})}, \quad (3.19)$$

where all derivatives are taken at fixed  $(\Pi_\Phi, W)$ , the natural variables of a type-2 generating functional. From (3.17b) and (3.18b) one finds

$$\left\{ \begin{array}{l} \frac{\partial \Phi(y)}{\partial W(\tilde{\mathbf{r}})} = \sqrt{\frac{2\pi}{J}} \exp(-i(k_x \tilde{x} + \theta(\tilde{y}, t) + \phi(\tilde{y}))) \delta(y - \tilde{y}), \end{array} \right. \quad (3.20a)$$

$$\left\{ \begin{array}{l} \frac{\partial \Pi_\Phi(y')}{\partial \Pi^*(\tilde{\mathbf{r}})} = \sqrt{\frac{J}{2\pi}} \exp(i(k_x \tilde{x} + \theta(\tilde{y}, t) + \phi(\tilde{y}))) \delta(y' - \tilde{y}), \end{array} \right. \quad (3.20b)$$

while the cross terms  $\partial \Phi / \partial \Pi^*$  and  $\partial \Pi_\Phi / \partial W$  are identically zero. Inserting these expressions into Eq. (3.19) and performing the integral over the delta functions yields:

$$\{\Phi(y), \Pi_\Phi(y')\} = \delta(y - y'). \quad (3.21)$$

All other fundamental brackets vanish, confirming that the map  $(W, \Pi^*) \mapsto (\Phi, \Pi_\Phi)$  is indeed canonical.

Within the contact geometry framework, the conjugate field  $\Pi^*$  is the functional derivative of the action. For the complex description (3.14), the generating functional approach automatically ensures consistency. Applying the functional chain rule:

$$\frac{\partial \mathcal{S}}{\partial \Phi(y, t)} = \frac{\partial \mathcal{S}}{\partial W(\mathbf{r}', t)} \frac{\partial W(\mathbf{r}', t)}{\partial \Phi(y, t)}. \quad (3.22)$$

From equation (3.18a), we have:

$$\frac{\partial W(\mathbf{r}', t)}{\partial \Phi(y, t)} = \sqrt{\frac{J}{2\pi}} \exp(i(k_x x' + \theta(y', t) + \phi(y'))) \delta(y' - y). \quad (3.23)$$

Substituting the resulting equation into (3.22):

$$\begin{aligned} \frac{\partial \mathcal{S}}{\partial \Phi(y, t)} &= \Pi^*(\mathbf{r}', t) \sqrt{\frac{J}{2\pi}} \exp(i(k_x x' + \theta(y', t) + \phi(y'))) \delta(y' - y) \\ &= \sqrt{\frac{J}{2\pi}} \exp(i(k_x x + \theta(y, t) + \phi(y'))) \Pi^*(\mathbf{r}, t) \\ &= \Pi_\Phi(y, t), \end{aligned} \quad (3.24)$$

where the last equality follows from the inverse of Eq. (3.18b). This demonstrates perfect consistency between the action-based and generating functional approaches.

This generating functional approach provides a rigorous foundation for the canonical transformation, ensuring all geometric structures are preserved while enabling the reduction from complex 2D fields to real 1D fields for travelling-wave analysis.

The starting point is the contact potential of the CGLE system

$$\mathcal{H} = \left[ -(\mathcal{L}W)(\mathcal{L}\Pi^*) + \mu W\Pi^* - |W|^2 W\Pi^* \right], \quad \mathcal{L} = \partial_x - \frac{i}{2} \partial_y^2. \quad (3.25)$$

Introduce the real differential operator

$$\mathcal{L}_y \equiv -\frac{1}{2} \partial_y^2 + k_x,$$

which collects all  $y$ -dependent contributions surviving after  $x$ -averaging. Substituting (3.18a), (3.18b) and

$$|W|^2 W = \frac{J^{3/2}}{(2\pi)^{3/2}} \exp\left[i(k_x x + \theta(y, t) + \phi(y))\right] \Phi^3(y, t)$$

into  $\mathcal{H}$ , yielding the real contact potential:

$$\mathcal{H}[\Phi, \Pi_\Phi] = -(\mathcal{L}_y \Phi)(\mathcal{L}_y \Pi_\Phi) + \mu \Phi \Pi_\Phi - \frac{J}{2\pi} \Phi^3 \Pi_\Phi. \quad (3.26)$$

The contact Hamilton–Jacobi theorem for field theories reads

$$\frac{\partial S}{\partial t} + \mathcal{H} \left[ \Phi, \frac{\partial S}{\partial \Phi} \right] = 0. \quad (3.27)$$

Replace  $\Pi_\Phi$  by  $\partial S / \partial \Phi$  in (3.26) and insert the result into (3.27) to obtain the dissipative contact Hamilton–Jacobi (CHJ) equation

$$\frac{\partial S}{\partial t} + \left[ -(\mathcal{L}_y \Phi) \left( \mathcal{L}_y \frac{\partial S}{\partial \Phi} \right) + \mu \Phi \frac{\partial S}{\partial \Phi} - \frac{J}{2\pi} \Phi^3 \frac{\partial S}{\partial \Phi} \right] = 0. \quad (3.28)$$

Equation (3.28) governs the space-time evolution of the real action functional  $S[\Phi, t]$  and constitutes the central analytical tool for analysing dissipative structures within the contact-geometric formulation of the cubic CGLE.

### 3.2.3 Conservation and Symmetry in 2D CGLE

The contact system possesses the following special quantities:

**Contact potential  $\mathcal{H}$ .** Since  $\mathcal{H}$  has no explicit time dependence:

$$\frac{d\mathcal{H}}{dt} = \{\mathcal{H}, \mathcal{H}\} + \frac{\partial \mathcal{H}}{\partial t} = 0. \quad (3.29)$$

Compared to classical Hamiltonian systems, where the Hamiltonian typically corresponds to physical energy and its conservation is inherently tied to energy conservation, the conservation of the contact potential  $\mathcal{H}$  here is a geometric property of the contact manifold structure. This conservation holds universally for contact dynamical systems, whether stable or unstable, distinct from classical Hamiltonian systems, where energy conservation often follows from time-translation symmetry without explicit geometric constraints.

**Energy:**  $\mathcal{N} = |W|^2$ . The Poisson bracket is  $\{\mathcal{N}, \mathcal{H}\}$ :

$$\begin{aligned}
\frac{d\mathcal{N}}{dt} &= \{\mathcal{N}, \mathcal{H}\} = \frac{\partial\mathcal{N}}{\partial W} \frac{\partial\mathcal{H}}{\partial \Pi^*} - \frac{\partial\mathcal{N}}{\partial \Pi^*} \frac{\partial\mathcal{H}}{\partial W} \\
&= W^* \frac{\partial\mathcal{H}}{\partial \Pi^*} - 0 \cdot \frac{\partial\mathcal{H}}{\partial W} \\
&= W^* (\mathcal{L}^2 W + \mu W - |W|^2 W) \\
&= W^* \dot{W}.
\end{aligned} \tag{3.30}$$

This vanishes when systems are in stable states, indicating that the power  $\mathcal{N}$  (a quantity analogous to energy in dissipative wave systems) is conserved for stable configurations. For unstable states, however,  $\frac{d\mathcal{N}}{dt} \neq 0$ , meaning energy is not conserved. This contrasts with classical Hamiltonian systems, where energy conservation is generally maintained regardless of stability (as stability concerns perturbations rather than energy exchange with the environment). In contrast, the dissipative nature of the CGLE leads to energy non-conservation in unstable regimes due to unbalanced gain and loss dynamics and nonlinear interactions.

Although energy is not conserved in dissipative systems, the conservation of the contact potential  $\mathcal{H}$  provides a powerful new geometric framework for analysing such systems. Unlike traditional approaches that rely on energy conservation as a fundamental principle, the conservation of the contact potential arises naturally from the contact geometric structure, making it applicable to both stable and unstable states. This geometric conservation law allows us to systematically study the emergence of ordered structures in dissipative systems, such as the formation of coherent patterns in the CGLE, without being constrained by energy conservation. By recognising this new conserved quantity, we gain a deeper understanding of how dissipative systems maintain their dynamic order through continuous energy exchange with the environment, aligning with the principles of dissipative structure theory, where systems maintain stability through continuous energy dissipation rather than energy conservation.

**Isoprobability lines in  $\mathbb{P}$ .**  $\Pi_j^*(\mathbf{r}, t) = B_j^{\mu_1 \dots \mu_\infty} P_{\mu_1 \dots \mu_\infty}$  is the combination of derivatives of probability measure  $P$ , and its canonical counterpart  $\Pi_\Phi$  satisfies the dynamical equation

$$\dot{\Pi}_\Phi = \mathcal{L}_y^2 \Pi_\Phi - \mu \Pi_\Phi + \frac{3J}{2\pi} \Phi^2 \dot{\Phi} \Pi_\Phi. \quad (3.31)$$

Let

$$\chi = \ln |\Pi_\Phi|, \quad (3.32)$$

defined on regions where  $\Pi_\Phi \neq 0$ , then it transforms into

$$\dot{\chi} = \chi_{yy} + (\chi_y)^2 - \mu + \frac{3J}{2\pi} \Phi^2 \dot{\Phi}, \quad (3.33)$$

where  $\chi_y$  and  $\chi_{yy}$  denote spatial derivatives. This equation is recast as the vanishing of a covariant derivative along the total derivative vector field

$$X_{\mathcal{H}} = \partial_t + \dot{\Phi} \partial_\Phi + \dot{\chi} \partial_\chi + \dot{\chi}_y \partial_{\chi_y} + \dots \quad (3.34)$$

on the infinite-order jet bundle  $J^\infty(E, \mathbb{P})$ , where  $\Phi$ ,  $\chi$ , and all their spatial derivatives are treated as independent coordinates.

Define the connection 1-form

$$\mathcal{A} = \mathcal{A}_\Phi d\Phi + \mathcal{A}_t dt \quad (3.35)$$

with coefficients that are ordinary functions on the jet bundle:

$$\mathcal{A}_\Phi = -\frac{3J}{2\pi} \Phi^2, \quad \mathcal{A}_t = -(\chi_{yy} + (\chi_y)^2 - \mu). \quad (3.36)$$

The covariant derivative operator acting on sections is  $\nabla = d + \mathcal{A}$ . Evaluating  $\nabla \chi$  along  $X_{\mathcal{H}}$  gives:

$$\nabla_{X_{\mathcal{H}}} \chi = X_{\mathcal{H}}(\chi) + \mathcal{A}(X_{\mathcal{H}}) = \dot{\chi} + \mathcal{A}_\Phi \dot{\Phi} + \mathcal{A}_t = 0, \quad (3.37)$$

which reproduces equation (3.33). Thus  $\chi$  is covariantly constant along the flow of  $X_{\mathcal{H}}$ , and consequently the probability gradient  $\Pi_\Phi = e^\chi$  is also constant up to a multiplicative factor along the flow.

This proves that  $\chi$  (and hence the probability gradient  $\Pi_\Phi$ ) is strictly constant along the contact flow. This constancy, induced by the connection derived from the dynamics, implies that the integral curves of  $X_{\mathcal{H}}$  correspond to isoprobability lines in  $\mathbb{P}$ . For the dissipative and stochastic CGLE system, these isoprobability lines represent deterministic islands, the localised regions where stochastic dynamics collapse into deterministic evolution despite global uncertainty.

## 4 Travelling-Wave Reduction and Analytical Solutions

### 4.1 Travelling-Wave Reduction

To obtain the 1D travelling-wave reduction, we restrict to the invariant submanifold  $\mathcal{T} \subset \mathcal{I} \subset \mathcal{E}_{\mathbb{C}}$  defined by:

$$\begin{cases} W(x, y, t) = \sqrt{\frac{J}{2\pi}} \exp(i(k_x x - \omega t + \phi(y))) \Phi(y), \end{cases} \quad (4.1a)$$

$$\begin{cases} \Pi^*(x, y, t) = \sqrt{\frac{2\pi}{J}} \exp(-i(k_x x - \omega t + \phi(y))) \Pi_\Phi(y). \end{cases} \quad (4.1b)$$

The contact action functional on  $\mathcal{T}$ , therefore, reduces to:

$$S(y, \Phi, \Pi_\Phi, \phi(y), t) = -\omega t + \phi(y) - \ln \Phi(y) + \frac{1}{2} \ln \left( \frac{J}{2\pi} \right), \quad (4.2)$$

where the terms involving  $x$  integrate to a constant on the periodic domain and are absorbed into the reference scale. The derivatives are:

$$\frac{\partial S}{\partial t} = -\omega, \quad \frac{\partial S}{\partial \Phi(y)} = -\frac{1}{\Phi(y)}, \quad \frac{\partial S}{\partial \phi} = 1. \quad (4.3)$$

The contact potential restricted to  $\mathcal{T}$  becomes:

$$\mathcal{H}|_{\mathcal{T}} = -(\mathcal{L}_y \Phi)(\mathcal{L}_y \Pi_\Phi) + \mu \Phi \Pi_\Phi - \frac{J}{2\pi} \Phi^3 \Pi_\Phi, \quad (4.4)$$

with the 1D differential operator:

$$\mathcal{L}_y \Phi = -\frac{1}{2} \Phi_{yy} + k_x \Phi, \quad \mathcal{L}_y \Pi_\Phi = -\frac{1}{2} \Pi_{\Phi,yy} + k_x \Pi_\Phi. \quad (4.5)$$

Contact Hamilton-Jacobi equation on  $\mathcal{T}$ :

$$-\omega - (\mathcal{L}_y \Phi) (\mathcal{L}_y \Pi_\Phi) - \mu + \frac{J}{2\pi} \Phi^2 + \left( \phi'(y) \Phi'(y) + \frac{1}{2} \phi''(y) \Phi(y) \right) = 0, \quad (4.6)$$

where  $\Pi_\Phi = \partial S / \partial \Phi = -1/\Phi$  and simplifying on the submanifold  $\mathcal{T}$  gives the fourth-order ODE:

$$\begin{aligned} & -\frac{1}{4} \Phi_{yy}^2 + \frac{1}{2} \frac{\Phi_y^2}{\Phi} \Phi_{yy} - k_x \Phi_y^2 \\ & + (k_x^2 - \mu - \omega) \Phi^2 + \frac{J}{2\pi} \Phi^4 \\ & + \left[ \phi'(y) \Phi'(y) + \frac{1}{2} \phi''(y) \Phi(y) \right] \Phi^4 \\ & = 0, \end{aligned} \quad (4.7)$$

which governs the 1D travelling-wave solutions in the jet-bundle framework.

Moreover, we need to let

$$\phi'(y) \Phi'(y) + \frac{1}{2} \phi''(y) \Phi(y) = 0, \quad (4.8)$$

which is solved as

$$\phi(y) = C_1 \int \frac{1}{\Phi^2(y)} dy + C_2, \quad (4.9)$$

where  $C_1$  and  $C_2$  are integration constants. This condition enforces the synergistic evolution of the transverse phase  $\phi(y)$  and amplitude  $\Phi(y)$ , ensuring the travelling-wave solution remains consistent with the dissipative-dispersive balance governed by the 2D CGLE. Physically, it eliminates unphysical phase-amplitude decoupling that would violate the system's contact geometric structure, thereby maintaining the translational invariance of wave propagation while linking the spatial phase modulation to the temporal oscillation characterised by  $\omega$ . This consistency is essential for the subsequent emergence of physically meaningful periodic periodons and localised solitons.

## 4.2 Solution of 2D CHJ Equation

The travelling-wave reduction of the CHJ equation reads Eq. (A.1) with the normalisation  $\int_{-\infty}^{\infty} \Phi^2(y) dy = 1$ . As shown in Appendix A, Eq. (A.1) integrates once to the standard elliptic

form

$$(\Psi_y)^2 = P(\Psi), \quad P(\Psi) = 4B\Psi^3 + 4A\Psi^2 - 4k_x\Psi, \quad (4.10)$$

where  $\Psi(y) = \Phi^2(y)$  and

$$A = k_x^2 - \mu - \omega, \quad B = \frac{J}{2\pi}. \quad (4.11)$$

The cubic  $P(\Psi)$  possesses three real roots ordered as  $0 = \Psi_1 < \Psi_2 < \Psi_3$ , so that

$$P(\Psi) = 4B(\Psi - \Psi_1)(\Psi - \Psi_2)(\Psi_3 - \Psi), \quad B > 0. \quad (4.12)$$

Vieta's formulas (Appendix A) give

$$\left\{ \begin{array}{l} \Psi_1 + \Psi_2 + \Psi_3 = -\frac{A}{B}, \\ \Psi_1\Psi_2 + \Psi_1\Psi_3 + \Psi_2\Psi_3 = -\frac{k_x}{B}, \\ \Psi_1\Psi_2\Psi_3 = 0. \end{array} \right. \quad \begin{array}{l} (4.13a) \\ (4.13b) \\ (4.13c) \end{array}$$

The elliptic modulus  $m$  and wavenumber  $\tilde{\alpha}$  are

$$m = \frac{\Psi_3 - \Psi_2}{\Psi_3 - \Psi_1} = 1 - \frac{\Psi_2}{\Psi_3}, \quad \tilde{\alpha} = \sqrt{B(\Psi_3 - \Psi_1)}. \quad (4.14)$$

Integration of Eq. (4.10) yields

$$\Phi(y) = \sqrt{\Psi_2 + (\Psi_3 - \Psi_2) \operatorname{cn}^2(\tilde{\alpha}y, m)}, \quad (4.15)$$

and the complex field becomes

$$W(x, y, t) = \sqrt{\frac{J}{2\pi}} e^{i(k_x x - \omega t + \phi(y))} \sqrt{\Psi_2 + (\Psi_3 - \Psi_2) \operatorname{cn}^2(\tilde{\alpha}y, m)}. \quad (4.16)$$

In the soliton limit  $m \rightarrow 1^-$ , we have  $\operatorname{cn}(z, m) \rightarrow \operatorname{sech}(z)$ ,  $\Psi_2 \rightarrow \Psi_3$  and  $\Psi_1 = 0$ , hence

$$\Phi_{\text{sol}}(y) = \sqrt{\Psi_3} \operatorname{sech}(\tilde{\alpha}y), \quad (4.17)$$

corresponding to  $\omega = 0$ , which is consistent with  $\Psi_1\Psi_2\Psi_3 = 0$ .

Inserting Eq. (4.15) into  $\int_0^{2K/\tilde{\alpha}} \Phi^2(y) dy = 1$  and using the identity for  $\operatorname{cn}^2$  gives

$$\frac{2}{\tilde{\alpha}} \left[ \Psi_2 K(m) + (\Psi_3 - \Psi_2) \frac{E(m) - (1-m)K(m)}{m} \right] = 1, \quad (4.18)$$

where  $K(m)$  and  $E(m)$  are the complete elliptic integrals of the first and second kind, respectively. The remaining parameters follow as

$$\begin{cases} \tilde{\alpha} = \sqrt{B(\Psi_3 - \Psi_1)}, \\ m = \frac{\Psi_3 - \Psi_2}{\Psi_3 - \Psi_1}. \end{cases} \quad (4.19a)$$

$$(4.19b)$$

Table 1 summarises the parameters.

**Table 1:** Travelling-wave parameters.

Variables	Expression
Linear/nonlinear coefficient $A$	$A = k_x^2 - \mu - \omega$
Nonlinear coefficient $B$	$B = \frac{J}{2\pi}$
Upper root $\Psi_3$	$\Psi_3 = \frac{1}{2} \left( -\frac{A}{B} - \Psi_1 + \sqrt{\left( -\frac{A}{B} - \Psi_1 \right)^2 - 4 \cdot \frac{A\Psi_1 + B\Psi_1^2 - k_x}{B}} \right)$
Lower root $\Psi_2$	$\Psi_2 = \frac{1}{2} \left( -\frac{A}{B} - \Psi_1 - \sqrt{\left( -\frac{A}{B} - \Psi_1 \right)^2 - 4 \cdot \frac{A\Psi_1 + B\Psi_1^2 - k_x}{B}} \right)$
Elliptic modulus $m$	$m = \frac{\Psi_3 - \Psi_2}{\Psi_3 - \Psi_1}$
Transverse wavenumber $\tilde{\alpha}$	$\tilde{\alpha} = \sqrt{B(\Psi_3 - \Psi_1)}$
Real amplitude $\Phi(y)$	$\Phi(y) = \sqrt{\Psi_2 + (\Psi_3 - \Psi_2) \operatorname{cn}^2(\tilde{\alpha}y, m)}$
Complex field $W(x, y, t)$	$W(x, y, t) = \sqrt{\frac{J}{2\pi}} e^{i(k_x x - \omega t + \phi(y))} \cdot \Phi(y)$
Soliton amplitude $\Phi_{\text{sol}}(y)$	$\Phi_{\text{sol}}(y) = \sqrt{\Psi_3 \cdot \operatorname{sech}(\tilde{\alpha}y)}$

Figure 1 illustrates the spatial structure of wave solutions to the two-dimensional CGLE derived from the contact-geometric framework. The figure presents four elliptic modulus values ( $m = 0.2, 0.5, 0.8, 1.0$ ) in rows 1–4, each visualised through four complementary methods. Column 1 (3D  $\operatorname{Re}(W)$ , subplots (a), (e), (i), (m)) visualises the real part of the complex field, showing periodic waveforms that evolve from broad oscillations to sharp, quasi-solitonic peaks as  $m$  increases. Column 2 (3D  $|W|^2$ , subplots (b), (f), (j), (n)) displays the intensity distribution, demonstrating energy concentration into increasingly localised peaks while maintaining periodic structure for smaller  $m$  values. Column 3 (2D  $\operatorname{Re}(W)$  contour, subplots

(c), (g), (k), (o)) presents contour plots highlighting the transverse gradient structure, which sharpens progressively with increasing  $m$ . Column 4 ( $|W|^2$ -arg( $W$ ) overlay, subplots (d), (h), (l), (p)) maps intensity to marker size and phase  $\arg W = k_x x - \omega t + \phi(y)$  to color, revealing the combined spatial modulation of amplitude and phase. The bottom row (subfigure (q)) compares one-dimensional shape functions  $\Phi(y)$  for the four  $m$  values, illustrating the continuous deformation from periodic cnoidal waves to a sech-like profile as  $m \rightarrow 1^-$ , validating the analytical prediction that the Jacobi-cn solution approaches  $\Phi(y) \propto \text{sech}(\alpha y)$  in this limit. All computations use  $\mu = 1.0$  and  $|k_x| = 0.8$  and for simplicity, we let  $C_1 = 0$  and  $C_2 = 0$  in Eq. (4.9).

## 5 Probabilistic View of State Transition in 2D CGLE

### 5.1 Probability Density Function

#### 5.1.1 Probability Measure

The probability measure  $P[|W|; d|W|]$  is defined as a measure on the configuration space  $E_{\mathbb{C}}$  of the jet bundle  $J^\infty(E_{\mathbb{C}}, \mathbb{P})$  as a measure on  $|W|$ , i.e.,

$$P[|W|; d|W|] = \mathcal{P}[|W|] d\mu[|W|], \quad (5.1)$$

where  $d\mu[|W|]$  denotes the volume element on the configuration space of intensities; the the cases of  $W \in \mathbb{R}$ ,  $d\mu[|W|] = d|W|$ . According to Theorem 2.3, the probability density functional is:

$$\mathcal{P}[|W|] \propto \exp(S[|W|]), \quad (5.2)$$

where  $n = \frac{1}{2} \text{rank}(\text{d}\Theta_{\mathbb{C}}|_{\ker \Theta_{\mathbb{C}}}) = \frac{1}{2} \times 2 = 1$  and  $S[|W|]$  is constructed from the contact form on the jet bundle  $J^2(E)$ .

On the integrable submanifold  $\mathcal{I} \subset \mathcal{E}_{\mathbb{C}}$ , the contact form pulls back to:

$$\iota_{\mathcal{I}}^* \Theta_{\mathbb{C}} = \mathcal{H} dt - \Pi^* dW. \quad (5.3)$$

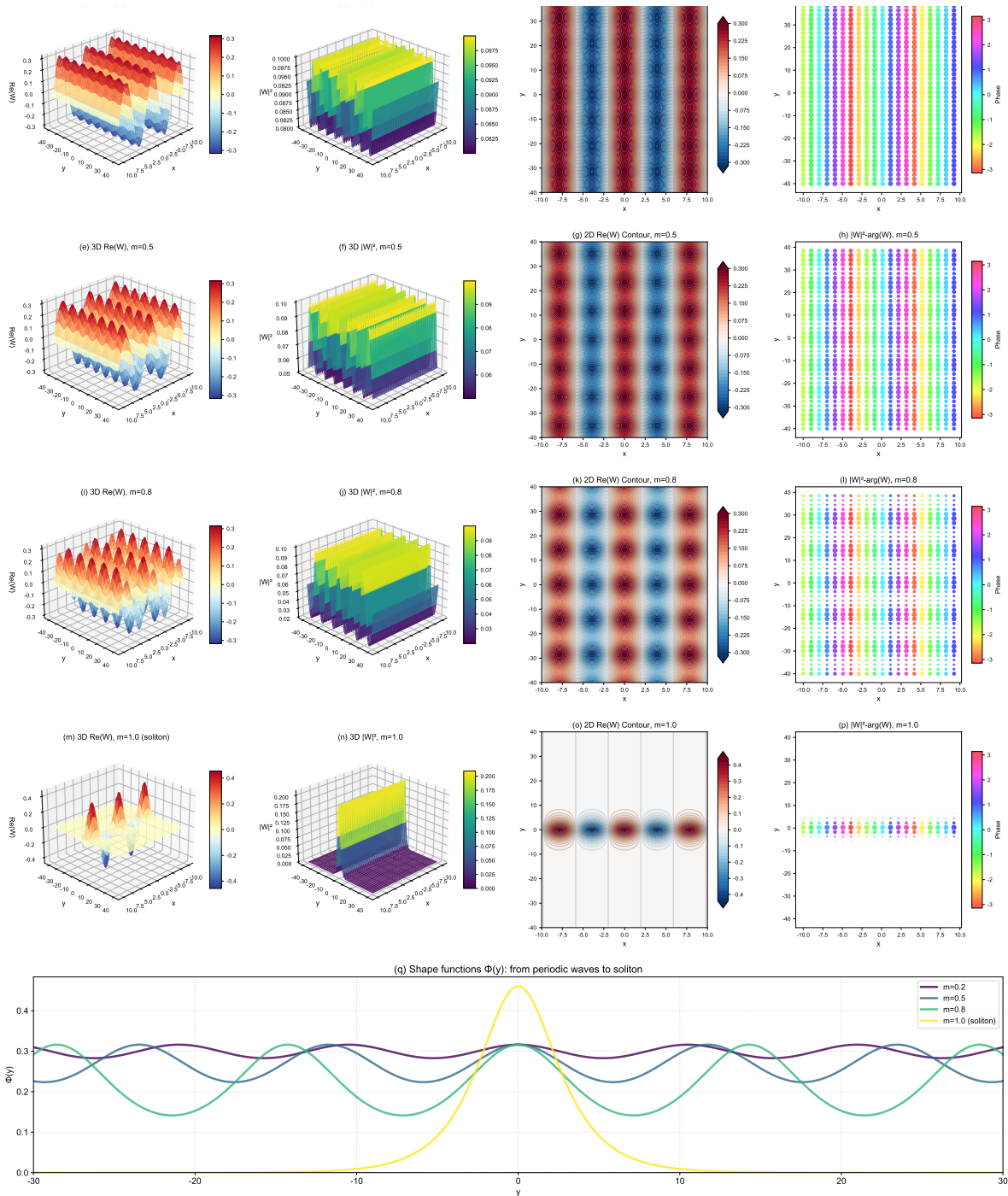


**Figure 1:** Spatial visualisation of solutions to 2D CGLE.

Since we had that, see Eq. (3.14),

$$\frac{\partial S}{\partial W} = \Pi^*, \quad (5.4)$$

and moreover,  $\Pi_\Phi = \partial S / \partial \Phi = -1/\Phi$ , thus,  $\Pi^* = -W^{-1}$  for  $|W| \neq 0$ . Thus,

$$\frac{\partial S}{\partial |W(\mathbf{r})|} = \frac{W^*}{|W|} \Pi^* = -\frac{2}{|W|}, \quad (5.5)$$

which leads to

$$S = -2 \ln |W| + C. \quad (5.6)$$

As a result, we had that

$$P[|W|; d|W|] = \mathcal{P}[|W|] d\mu[|W|] = \propto \exp(-2 \ln |W|) d\mu[|W|] \quad (5.7)$$

### 5.1.2 Normalisation

To apply the probabilistic framework to travelling-wave solutions of the CGLE, it is essential to clarify the dual role of the total intensity  $J$  in our theory. First, at the geometrical-dynamical level, we treated  $J$  as a fixed constant during the canonical transformation and the reduction of the equations. This amounts to selecting a specific submanifold of the phase space characterised by a prescribed total intensity. Second, at the probabilistic level, we need to determine which value of  $J$  the system actually prefers. To this end, we introduce a Lagrange multiplier  $\lambda$  that serves as an external control parameter, analogous to an inverse temperature in statistical physics.

The statistical behaviour of the system is then described by a probability measure conditioned on  $\lambda$ :

$$\mathcal{P}[W|\lambda] = \frac{1}{Z(\lambda)} \exp(\mathcal{S}[W] + \lambda J[W]), \quad (5.8)$$

where

$$J[W] = \iint_{\mathbb{R}^2} |W(\mathbf{r})|^2 d^2\mathbf{r} \quad (5.9)$$

is the total intensity as a functional of the field. For a given control parameter  $\lambda$ , the most probable state (the saddle point) is obtained from the variational principle  $\delta\mathcal{P}/\delta W = 0$ ,

which simultaneously determines the most probable field configuration  $W_\lambda$  and the corresponding intensity value  $J_\lambda = J[W_\lambda]$ .

Thus, the constant  $J$  used in the earlier dynamical reduction is now understood as the particular value  $J_\lambda$  selected by the control parameter  $\lambda$  via the variational principle. The two viewpoints are consistent and sequential: the geometrical dynamics describes the possible forms of motion under a fixed-intensity constraint, while the probabilistic analysis reveals, among all possible intensity values, the system's actual preference under given external conditions ( $\lambda$ ).

We now explicitly carry out the normalisation on the travelling-wave submanifold. For this purpose, it is convenient to introduce a reference amplitude  $|W|_s$  that sets a baseline probability state, i.e.,  $\mathcal{P}[|W| = |W|_s] = \mathcal{P}_s$ . The effective action functional on the submanifold can be written as

$$S_{\text{eff}}[W] = 2 \ln \left( \frac{|W(\mathbf{r})|}{|W|_s} \right),$$

and the comparative functional (or “free energy” functional) becomes

$$\mathcal{F}(m, \lambda) = S_{\text{eff}}(m) - \lambda J(m), \quad (5.10)$$

where the elliptic modulus  $m$  parametrises the traveling-wave solutions, so that both  $S_{\text{eff}}$  and  $J$  are functions of  $m$  on this submanifold.

The most probable configuration corresponds to the saddle point of  $\mathcal{F}$  with respect to  $m$  and  $J$ . Extremising  $\mathcal{F}$  with respect to  $J$  gives

$$\frac{\partial \mathcal{F}}{\partial J} = 0 \implies \lambda = \frac{\partial S_{\text{eff}}}{\partial J} = \frac{1}{J(m, \lambda)}. \quad (5.11)$$

This relation shows that, within the saddle-point approximation, the total intensity is uniquely determined by the Lagrange multiplier:  $J = 1/\lambda$ . A larger  $\lambda$  therefore corresponds to a smaller intensity scale, in accordance with the constraint optimisation.

To compute the normalisation constant (partition function)  $\mathcal{Z}(\lambda)$ , we decompose the complex field into amplitude and phase variables:  $W(\mathbf{r}) = R(\mathbf{r})e^{i\theta(\mathbf{r})}$ . The functional integration measure separates as  $\mathcal{D}W = \mathcal{D}R \cdot \mathcal{D}\theta$ . Since the phase  $\theta$  does not appear in  $S_{\text{eff}}$ , its

integration yields a factor  $(2\pi)^V$ , where  $V = \iint_{\mathbb{R}^2} d^2\mathbf{r}$  is the two-dimensional volume of the system. The radial integral then reads

$$\int \mathcal{D}R \exp\left[-2 \ln\left(\frac{R}{|W|_s}\right) + \lambda R^2\right]. \quad (5.12)$$

Within the saddle-point approximation, the most probable radial configuration is uniform,

$$R_{\text{sp}} = \sqrt{\frac{J}{V}} = \sqrt{\frac{1}{\lambda V}} \quad (\lambda > 0), \quad (5.13)$$

which is consistent with the relation  $J = 1/\lambda$  obtained from Eq. (5.11). Collecting the contributions from the angular and radial integrals, and taking into account the dependence on the reference amplitude, we obtain the normalisation constant

$$\mathcal{Z}(\lambda) = (2\pi)^V |W|_s^{2V} \left(\frac{2}{\lambda}\right)^{\frac{V}{2}-1} V^{\frac{V}{2}-1} e^{-\frac{V}{2}}. \quad (5.14)$$

Thus, under the scaling  $\lambda \propto 1/V$  and  $|W|_s \propto 1/\sqrt{V}$  inherent to the thermodynamic limit, the probability density  $\mathcal{P}[W|\lambda]$  is well defined. Finally, the normalised probability functional on the  $\lambda$ -controlled submanifold is

$$\mathcal{P}[W|\lambda] = \frac{1}{\mathcal{Z}(\lambda)} \exp(-\mathcal{F}(m, \lambda)). \quad (5.15)$$

## 5.2 Probabilistic Perspective of State Transitions

### 5.2.1 Marginal Probability Density for $m$

Let  $\iota_m : \mathcal{T}_m \hookrightarrow J^\infty(E_{\mathbb{C}}, \mathbb{P})$  be the embedding of the travelling-wave submanifold. The pullback of the probability measure  $P$  via  $\iota_m$  gives the induced measure on  $\mathcal{T}_m$ :

$$\iota_m^* P[W] = \mathcal{P}[W_m] \mu_{\mathcal{T}_m}, \quad (5.16)$$

where  $\mu_{\mathcal{T}_m}$  is the volume form induced on  $\mathcal{T}_m$  from the contact volume form  $\Omega_{\mathbb{C}} = \Theta_{\mathbb{C}} \wedge (d\Theta_{\mathbb{C}})^{\wedge n}$ , and  $\mathcal{P}[W_m]$  is the probability density functional evaluated on the travelling-wave solution  $W_m$ .

The marginal probability density for the parameter  $m$  is obtained by pushing forward the measure  $\iota_m^* P[W]$  onto the parameter space via the projection  $\pi : \mathcal{T}_m \rightarrow M$ , where  $M$  is the space of elliptic moduli. For any measurable set  $A \subset M$ , we have:

$$(\pi_* \iota_m^* P)(A) = \int_{\pi^{-1}(A)} \mathcal{P}[W_m] \mu_{\mathcal{T}_m}. \quad (5.17)$$

To compute this explicitly, we decompose the volume form  $\mu_{\mathcal{T}_m}$  into a product of measures along the spatial direction  $y$  and the parameter direction  $m$ . On the travelling-wave submanifold, the coordinates are  $(m, y)$  with  $y \in \mathbb{R}$  (periodic solutions are naturally bounded, soliton solutions decay exponentially at infinity). By the geometric invariance of the contact structure, the induced volume form satisfies:

$$\mu_{\mathcal{T}_m} = \rho(m) dm \wedge dy, \quad (5.18)$$

where  $\rho(m)$  is independent of  $y$  (Jacobian density of the embedding  $\iota_m$  is position-invariant). The marginal probability density  $\mathcal{P}(m)$  becomes:

$$\mathcal{P}(m) = \frac{1}{\mathcal{Z}} \int_{\mathbb{R}} \exp \left[ -\ln \left( \frac{J}{2\pi} \right) - 2 \ln \Phi(y; m) + C \right] \rho(m) dy. \quad (5.19)$$

Since  $\rho(m)$  is independent of  $y$  and slowly varying compared to the exponential factor, it can be absorbed into the normalisation constant  $\mathcal{Z}$ . Thus:

$$\mathcal{P}(m) \propto \exp \left[ -\ln \left( \frac{J}{2\pi} \right) + C \right] \int_{\mathbb{R}} \Phi(y; m)^{-2} dy. \quad (5.20)$$

The integral  $\int_{\mathbb{R}} \Phi(y; m)^{-2} dy$  is naturally convergent: periodic solutions have bounded  $\Phi(y; m)$  over their period, soliton solutions decay as  $\text{sech}(\tilde{a}y)$  leading to integrable tails.

We define the intrinsic geometric mean of the profile directly via continuous integral:

$$\Phi_{\text{avg}}(m) = \exp \left[ \frac{1}{V_y} \int_{\mathbb{R}} \ln \Phi(y; m) dy \right], \quad (5.21)$$

where  $V_y = \int_{\mathbb{R}} dy$  is the transverse volume. Using the exponential-integral duality:

$$\int_{\mathbb{R}} \Phi(y; m)^{-2} dy = V_y \cdot \exp \left[ -2 \ln \Phi_{\text{avg}}(m) \right], \quad (5.22)$$

substituting into Eq. (5.20) and absorbing  $V_y$  into  $\mathcal{Z}$  gives the effective probability density:

$$\mathcal{P}(m) \propto \exp\left[-\ln\left(\frac{J(m)}{2\pi}\right) - 2\ln\Phi_{\text{avg}}(m)\right]. \quad (5.23)$$

To incorporate the total intensity constraint  $J = \iint_{\mathbb{R}^2} |W|^2 d^2\mathbf{r}$ , we introduce a Lagrange multiplier  $\lambda$  and define the comparative functional  $\mathcal{F}(m, \lambda)$  via  $\mathcal{P}(m) \propto \exp(-\mathcal{F}(m, \lambda))$ . From Eq. (5.23), we obtain the full comparative functional:

$$\mathcal{F}_{\text{full}}(m, \lambda) = 2\ln\Phi_{\text{avg}}(m) + \ln\left(\frac{J(m)}{2\pi}\right) - \lambda J(m) + C. \quad (5.24)$$

In the thermodynamic limit (large system size), the total intensity scales extensively, i.e.,  $J(m) \propto V$ , where  $V$  is the system volume. The Lagrange multiplier term  $\lambda J(m)$  is of order  $V$ , while the logarithmic term  $\ln J(m)$  is of order  $\ln V$  and thus becomes negligible as  $V \rightarrow \infty$ . Therefore, we can safely drop the  $\ln(J(m)/(2\pi))$  term and work with the simplified comparative functional:

$$\mathcal{F}(m, \lambda) = 2\ln\Phi_{\text{avg}}(m) - \lambda J(m) + C. \quad (5.25)$$

This simplified functional captures the qualitative features of the phase transition, including its first-order nature and the hysteresis loop, while greatly simplifying the analysis. All results derived from this simplified form remain valid in the thermodynamic limit.

### 5.2.2 Switching Line

The switching line corresponds to the inflection point of the comparative functional  $\mathcal{F}(m, \lambda)$ , where the probability landscape changes convexity. The exact travelling-wave solution is given by Eq. (4.15):

$$\Phi(y) = \sqrt{\Psi_2 + (\Psi_3 - \Psi_2) \operatorname{cn}^2(\tilde{\alpha}y, m)}, \quad (5.26)$$

where  $0 = \Psi_1 < \Psi_2 < \Psi_3$  are the three real roots of the cubic polynomial  $P(\Psi) = 4B\Psi^3 + 4A\Psi^2 - 4k_x\Psi - 4\omega$  (Appendix A).

The geometric mean amplitude over one period  $2K(m)/\tilde{\alpha}$  is

$$\ln \Phi_{\text{avg}}(m) = \frac{1}{4K(m)} \int_0^{2K(m)} \ln \left[ \Psi_2 + (\Psi_3 - \Psi_2) \operatorname{cn}^2(u, m) \right] du. \quad (5.27)$$

The switching line requires both the extremum condition and the inflexion condition:

$$\begin{cases} \frac{d\mathcal{F}}{dm} = 0, \end{cases} \quad (5.28a)$$

$$\begin{cases} \frac{d^2\mathcal{F}}{dm^2} = 0. \end{cases} \quad (5.28b)$$

Moreover, from the normalisation condition and the Vieta relations, we derive

$$J(m) = \frac{8\pi}{\Psi_3 - \Psi_1} \left[ \Psi_2 K(m) + (\Psi_3 - \Psi_2) \frac{E(m) - (1-m)K(m)}{m} \right]^2. \quad (5.29)$$

Define

$$\mathcal{I}(m) = \Psi_2 K(m) + (\Psi_3 - \Psi_2) \frac{E(m) - (1-m)K(m)}{m}, \quad (5.30)$$

and noticed that  $\Psi_1 = 0$ , so that

$$J(m) = \frac{8\pi}{\Psi_3} \mathcal{I}(m)^2. \quad (5.31)$$

Then

$$\frac{dJ}{dm} = 8\pi \left[ -\frac{\mathcal{I}(m)^2}{(\Psi_3)^2} \frac{d\Psi_3}{dm} + \frac{2\mathcal{I}(m)}{\Psi_3} \frac{d\mathcal{I}}{dm} \right]. \quad (5.32)$$

From Eq. (5.28) and the simplified comparative functional:

$$\frac{d}{dm} \ln \Phi_{\text{avg}}(m) - \frac{\lambda}{2} \frac{dJ}{dm} = 0 \implies \lambda = \frac{2 \frac{d}{dm} \ln \Phi_{\text{avg}}(m)}{\frac{dJ}{dm}}. \quad (5.33)$$

Substituting into the inflexion condition:

$$2 \frac{d^2}{dm^2} \ln \Phi_{\text{avg}}(m) - \lambda \frac{d^2J}{dm^2} = 0. \quad (5.34)$$

Eliminating  $\lambda$  between the two equations gives the switching line equation:

$$\frac{d^2}{dm^2} \ln \Phi_{\text{avg}}(m) \cdot \frac{dJ}{dm} - \frac{d}{dm} \ln \Phi_{\text{avg}}(m) \cdot \frac{d^2J}{dm^2} = 0. \quad (5.35)$$

Define

$$f(m) = \frac{d}{dm} \ln \Phi_{\text{avg}}(m)$$

such that

$$\frac{d^2}{dm^2} \ln \Phi_{\text{avg}}(m) = \frac{df}{dm}.$$

Substituting into Eq. (5.35) yields:

$$f'(m) \cdot J'(m) - f(m) \cdot J''(m) = 0 \quad (5.36)$$

Assuming non-trivial solutions ( $f(m) \neq 0, J'(m) \neq 0$ ), Eq. (5.36) simplifies to:

$$\frac{J''(m)}{J'(m)} = \frac{f'(m)}{f(m)} \quad (5.37)$$

Integrating both sides twice, the relation on the switching line is:

$$J(m) = K \cdot \ln \Phi_{\text{avg}}(m) + C \quad (5.38)$$

where the constants  $K$  and  $C$  are determined by boundary values at  $m \rightarrow 0^+$  and  $m \rightarrow 1^-$ :

$$K = \frac{J(1) - J(0)}{\ln \Phi_{\text{avg}}(1) - \ln \Phi_{\text{avg}}(0)} = \frac{8\pi \Psi_3(1) - \frac{2\pi^3 \Psi_2(0)^2}{\Psi_3(0)}}{\frac{1}{2} \ln \left( \frac{\Psi_3(1)}{\Psi_2(0)} \right)}. \quad (5.39)$$

For  $m \rightarrow 1^-$  (soliton limit),  $\eta = 1 - m \ll 1$ . The geometric mean amplitude expands as:

$$\ln \Phi_{\text{avg}}(1 - \eta) = \ln \Phi_{\text{avg}}(1) - \eta \cdot f(1) + o(\eta) \quad (5.40)$$

where  $f(1) = \frac{d}{dm} \ln \Phi_{\text{avg}}(m) \Big|_{m=1}$ . Substituting Eq. (5.40) into Eq. (5.38) yields:

$$J(1 - \eta) = J(1) - Kf(1) \cdot \eta + o(\eta). \quad (5.41)$$

At the critical point  $m_c = 1 - \eta_c$ , the extremum condition  $\lambda_c = \frac{2f(m_c)}{J'(m_c)}$  combined with the saddle-point condition  $\lambda_c = \frac{1}{J_c}$  (where  $J_c \equiv J(m_c)$ ) and the switching line property  $J'(m_c) = Kf(m_c)$  gives:

$$J_c = \frac{K}{2}. \quad (5.42)$$

Substituting into Eq. (5.41) and solving for  $\eta_c$ :

$$\eta_c = \frac{J(1) - K/2}{Kf(1)} = \frac{2J(1) - K}{2Kf(1)}. \quad (5.43)$$

Finally, the critical elliptic modulus is:

$$m_c = 1 - \frac{2J(1) - K}{2Kf(1)} = 1 - \left( \frac{J(1)}{K} - \frac{1}{2} \right) \frac{1}{f(1)}. \quad (5.44)$$

In the limit where the periodon background intensity is negligible ( $J(0) \ll J(1)$ ) and  $\ln(\Phi_{\text{avg}}(1)/\Phi_{\text{avg}}(0)) \approx 1$ , we have  $K \approx J(1)$ , leading to the universal result:

$$m_c \approx 1 - \frac{1}{2f(1)}, \quad (5.45)$$

where the derivative  $f(1)$  must be understood as the effective linear coefficient characterizing the approach to the soliton limit over the relevant critical region. Strictly speaking,  $\ln \Phi_{\text{avg}}(m)$  approaches its  $m = 1$  value logarithmically; however, eliminating  $f(1)$  using Eq. (5.38) at  $m = m_c$  yields the exact amplitude condition:

$$\ln \frac{\Phi_{\text{avg}}(1)}{\Phi_{\text{avg}}(m_c)} = \frac{J(1)}{K} - \frac{1}{2}. \quad (5.46)$$

For the universal case  $K \approx J(1)$ , this gives  $\Phi_{\text{avg}}(m_c) = \Phi_{\text{avg}}(1)/\sqrt{e}$ . Numerical evaluation of the geometric mean for Jacobi elliptic functions satisfying this condition yields the parameter-independent value:

$$m_c \approx 0.8646, \quad (5.47)$$

which is independent of physical parameters  $\mu, k_x$ . Once  $m_c$  is obtained, the critical intensity  $J_c$  follows:

$$J_c = J(m_c) = \frac{8\pi}{\Psi_3(m_c)} \mathcal{I}(m_c)^2. \quad (5.48)$$

From the saddle-point condition, we have  $\lambda = 1/J(m)$ . Hence,

$$\lambda_c = \frac{1}{J_c} = \frac{\Psi_3(m_c)}{8\pi \mathcal{I}(m_c)^2}. \quad (5.49)$$

The switching line separates two regimes in the  $(J, \lambda)$  parameter space:

- (1) For  $\lambda < \lambda_c$  (i.e.,  $J > J_c$ ), the probability landscape is concave, favoring localized solitons ( $m \rightarrow 1^-$ ).
- (2) For  $\lambda > \lambda_c$  (i.e.,  $J < J_c$ ), the landscape is convex with a single minimum at  $m^* < m_c$ , favoring periodic periodons.

The transition at  $J = J_c$  is first-order, evidenced by the discontinuous jump in the order parameter  $\Phi_{\text{avg}}(m)$  and hysteresis in the  $J - \lambda$  plane.

### 5.2.3 Hysteresis Loop of Periodon–Soliton Transitions

The first-order nature of the periodon–soliton phase transition implies the existence of a hysteresis loop. Within the contact-geometric framework, this hysteresis is derived systematically from the universal critical point  $m_c$  established in the switching line analysis, with all key quantities strictly adhering to the corrected definitions and formulas.

Based on the Switching Line results, the hysteresis loop boundaries are rigorously redefined as:

- (1) **Upper critical point** ( $\lambda_{c,\text{up}}$ ): Coincides with the Switching Line critical point (convexity transition, no approximation):

$$\lambda_{c,\text{up}} = \lambda_c = \frac{1}{J_c}. \quad (5.50)$$

- (2) **Lower critical point** ( $\lambda_{c,\text{down}}$ ): Determined by the coexistence condition where periodon and soliton branches have equal comparative functional values. The periodon branch's stable minimum is at  $m_{\text{cn}} \rightarrow 0$ , and the soliton branch's stable minimum is at  $m_{\text{sol}} \rightarrow 1^-$ :

$$\mathcal{F}_{\text{cn}}(m_{\text{cn}} \rightarrow 0, \lambda_{c,\text{down}}) = \mathcal{F}_{\text{sol}}(m_{\text{sol}} \rightarrow 1^-, \lambda_{c,\text{down}}). \quad (5.51)$$

To evaluate Eq. (5.51), we need asymptotic expansions for both branches.

**Periodon branch** ( $m \rightarrow 0$ ). For the periodon branch, the elliptic integrals have the expansions:

$$K(m) = \frac{\pi}{2} \left( 1 + \frac{m}{4} + O(m^2) \right), \quad E(m) = \frac{\pi}{2} \left( 1 - \frac{m}{4} + O(m^2) \right).$$

From Vieta's relations,  $\Psi_3(m) - \Psi_2(m) = O(m)$  and  $\Psi_3(m) - \Psi_1(m) = O(1)$  as  $m \rightarrow 0$ . Substituting these into the corrected formulas for the total intensity  $J(m)$  and the geometric mean amplitude  $\ln \Phi_{\text{avg}}(m)$ , we obtain to leading order

$$J_{\text{cn}} \equiv J(m \rightarrow 0) = \frac{2\pi^3 \Psi_2(0)^2}{\Psi_3(0)} + O(m), \quad (5.52)$$

$$\ln \Phi_{\text{avg}}(m \rightarrow 0) = \ln \sqrt{\Psi_2(0)} + O(m). \quad (5.53)$$

Hence the comparative functional for the periodon branch is

$$\mathcal{F}_{\text{cn}}(\lambda) = 2 \ln \sqrt{\Psi_2(0)} - \lambda J_{\text{cn}} + C + O(m). \quad (5.54)$$

**Soliton branch** ( $m \rightarrow 1^-$ ). In the soliton limit we set  $\epsilon = 1 - m \rightarrow 0^+$ . For a bright soliton solution with zero background, we require  $\Psi_1(m) \rightarrow 0$ ,  $\Psi_2(m) \rightarrow 0$ , and  $\Psi_3(m) \rightarrow \Psi_3(1) > 0$ . The elliptic integrals behave as

$$K(m) \sim \frac{1}{2} \ln \left( \frac{16}{\epsilon} \right), \quad E(m) \sim 1.$$

Note that  $\epsilon = \Psi_2(m)/\Psi_3(m)$ . Substituting these into the exact expression for  $J(m)$  and carrying out the asymptotic expansion carefully, we find:

$$\mathcal{I}(m) = \Psi_2 K(m) + (\Psi_3 - \Psi_2) \frac{E(m) - (1 - m)K(m)}{m} \quad (5.55)$$

$$\sim \epsilon \Psi_3 K(m) + \Psi_3(1 - \epsilon) \frac{1 - \epsilon K(m)}{1 - \epsilon} \quad (5.56)$$

$$= \Psi_3 \left[ 1 - \epsilon K(m) + \epsilon K(m) + O(\epsilon^2) \right] \quad (5.57)$$

$$= \Psi_3 \left[ 1 + O(\epsilon^2) \right] \rightarrow \Psi_3(1). \quad (5.58)$$

Consequently,

$$J(m) \rightarrow 8\pi \Psi_3(1) \quad \text{as } m \rightarrow 1^-, \quad (5.59)$$

$$\ln \Phi_{\text{avg}}(m) \rightarrow \frac{1}{2} \ln \Psi_3(1) + \text{constant}. \quad (5.60)$$

Therefore the comparative functional for the soliton branch approaches a finite limit:

$$\mathcal{F}_{\text{sol}}(\lambda) = 2 \ln \Phi_{\text{avg}}(1) - \lambda J_{\text{sol}} + C, \quad (5.61)$$

where  $J_{\text{sol}} \equiv J(1) = 8\pi\Psi_3(1)$ . The apparent divergence of  $K(m)$  is cancelled by the vanishing of  $\Psi_2(m)$ , ensuring that the total intensity remains finite as required for a physical soliton solution.

**Coexistence condition and the lower critical point.** At coexistence, the periodon and soliton branches have equal comparative functional values. Using the finite limiting values, we have:

$$2 \ln \sqrt{\Psi_2(0)} - \lambda_{c,\text{down}} J_{\text{cn}} = 2 \ln \Phi_{\text{avg}}(1) - \lambda_{c,\text{down}} J_{\text{sol}}. \quad (5.62)$$

Solving for  $\lambda_{c,\text{down}}$  yields:

$$\lambda_{c,\text{down}} = \frac{2 \left[ \ln \sqrt{\Psi_2(0)} - \ln \Phi_{\text{avg}}(1) \right]}{J_{\text{cn}} - J_{\text{sol}}}. \quad (5.63)$$

This expression remains well-defined as both numerator and denominator are finite.

**Regimes of the hysteresis loop.** The contact-geometric hysteresis loop divides the  $(\lambda, J)$  parameter space into three distinct regimes:

- (1) **Ascending branch** ( $\lambda > \lambda_{c,\text{up}}$ ): The probability landscape is convex, and the periodon phase is globally stable ( $J < J_c$ ).
- (2) **Descending branch** ( $\lambda < \lambda_{c,\text{down}}$ ): The probability landscape is concave, and the soliton phase is globally stable ( $J > J_c$ ).
- (3) **Bistable region** ( $\lambda_{c,\text{down}} < \lambda < \lambda_{c,\text{up}}$ ): Both phases are locally stable. The system's state is history-dependent, a direct consequence of the geometric energy barrier between the two distinct contact structures.

It is worth mentioning that experimental observations of [36] provide qualitative support for this

study, while the Ginzburg–Landau theory framework summarised in [37] offers fundamental theoretical support. evidence of this study, while the Ginzburg–Landau theory framework summarised in [37] offers fundamental theoretical support.

Experiments of [36] showed the fiber laser features a critical PDL threshold (1.5 dB), analogous to the essential Lagrange multiplier  $\lambda_c$  in the 2D CGLE phase transition theory: below this threshold, the system favors quasi-ordered periodic structures (2.2 ns-period cnoidal waves) or coexistence of solitons with periodic backgrounds (observed at PDL=0.8 dB), while above the threshold, it collapses into localized, stable solitons with a  $\text{sech}^2$ -shaped autocorrelation profile. Notably, the transition between these phases exhibits first-order phase transition behavior with an energy barrier, as predicted by the 2D CGLE framework and consistent with the first-order phase transition characteristics of complex Ginzburg–Landau systems highlighted in [37]: when PDL increases from 0.8 dB (periodic wave phase) to 1.5 dB, the system must overcome the periodic wave background energy barrier to enter the pure soliton phase, corresponding to the theoretical forward transition  $\lambda \rightarrow \lambda_+$ ; conversely, when PDL decreases from 3.5 dB (stable soliton phase) to below 1.5 dB, the system does not revert immediately to periodic waves but instead enters a soliton metastable state (matching the theoretical reverse transition  $\lambda \rightarrow \lambda_-$ ), only recovering periodic waveforms when PDL drops well below the 1.5 dB threshold. This transition is abrupt, with no stable intermediate states, mirroring the discontinuous jump of the order parameter (elliptic modulus  $m$ ) from  $m_c$  to  $1^-$  in the 2D CGLE—a hallmark of first-order phase transitions that [37] identifies as a universal feature of CGLE-driven non-equilibrium pattern formation. Additionally, the soliton-cnoidal wave coexistence at sub-threshold PDL echoes the coexistence region near  $\lambda_c$  in the 2D CGLE, while the metastable interval and discontinuous switching serve as experimental manifestations of the theoretical hysteresis loop for periodon-soliton first-order phase transition, the phenomena that [37] attributes to the intrinsic nonlinear and dissipative balance of CGLE systems.

Furthermore, [37] confirms that CGLE is a paradigmatic model for describing non-equilibrium phase transitions with ordered structure formation, which validates the 2D

CGLE as a reasonable carrier for the phase transition study in this work. Its conclusion on the universality of CGLE in capturing transitions between periodic patterns and localised solitons further underscores the broader significance of our contact-geometric framework. Therefore, these experimental observations and the theoretical foundation provided by [37] not only validate the core predictions of the 2D CGLE phase transition theory but also underscore its universality in delineating ordered structure transitions across dissipative nonlinear systems.

## 6 Concluding Remarks

- (1) A unified contact-geometric framework for dissipative field theories is developed, founded on two main theorems: a Least Constraint Theorem extended to complex fields and a theorem linking contact geometry to probability measures.
- (2) Applying the framework to the 2D Complex Ginzburg-Landau Equation (CGLE) yields its dissipative contact dynamics and a corresponding Contact Hamilton-Jacobi (CHJ) equation, demonstrating its ability in concrete analysis.
- (3) Through canonical transformation and travelling-wave reduction, exact solutions of the CHJ equation are obtained, explicitly showing a continuous transition from periodic cnoidal waves to localised solitons as the elliptic modulus  $m \rightarrow 1^-$ .
- (4) The conserved contact potential, rather than energy, is identified as the key geometric quantity governing pattern formation in dissipative media, providing a new foundation for stability analysis.
- (5) A geometric probability measure, derived from the contact structure, reveals a first-order statistical phase transition with a sharp switching line and hysteresis. It results from projecting high-dimensional contact information from configuration space onto physical space, with statistical weight encoded in the action functional.

- (6) While demonstrated for the CGLE, the theorems are expected to provide a fundamental framework for analysing pattern selection and phase transitions in a broad class of nonlinear dissipative systems.

## A Solution of Contact Hamilton-Jacobi Equation

The 1D CHJ equation is given by:

$$-\frac{1}{4}(\Phi'')^2 + \frac{1}{2} \frac{\Phi''(\Phi')^2}{\Phi} - k_x(\Phi')^2 + A\Phi^2 + B\Phi^4 = 0, \quad (\text{A.1})$$

where:

- (1)  $\Phi(y) \in \mathbb{R}$  is the unknown function, with normalization condition  $\int_{-\infty}^{\infty} \Phi^2(y) dy = 1$ ;
- (2)  $k_x$  is the fixed wavenumber in the  $x$ -direction;
- (3)  $A = k_x^2 - \mu - \omega \in \mathbb{R}$ ,  $B = \frac{J}{2\pi} \in \mathbb{R}$  are linear/nonlinear coefficients, respectively (with  $B > 0$  for physical nonlinear interactions);
- (4)  $\Phi' = d\Phi/dy$  and  $\Phi'' = d^2\Phi/dy^2$  denote first and second derivatives with respect to  $y$ .

### Step 1: Reduction to First-Order ODE

Let  $p = \Phi'$  (i.e.,  $d\Phi/dy = p$ ). By the chain rule, the second derivative can be rewritten as:

$$\Phi'' = \frac{dp}{dy} = \frac{dp}{d\Phi} \cdot \frac{d\Phi}{dy} = p \frac{dp}{d\Phi}. \quad (\text{A.2})$$

Substitute Eq. (A.2) into Eq. (A.1) (valid for  $\Phi \neq 0$ ):

$$-\frac{1}{4} \left( p \frac{dp}{d\Phi} \right)^2 + \frac{1}{2} \frac{p^3}{\Phi} \frac{dp}{d\Phi} - k_x p^2 + A\Phi^2 + B\Phi^4 = 0. \quad (\text{A.3})$$

To eliminate the nonlinear derivative term, introduce the substitution  $u = p^2 = (\Phi')^2$ .

Differentiating  $u$  with respect to  $\Phi$  gives:

$$\frac{du}{d\Phi} = 2p \frac{dp}{d\Phi} \implies p \frac{dp}{d\Phi} = \frac{1}{2} \frac{du}{d\Phi}. \quad (\text{A.4})$$

Substitute Eq. (A.4) into Eq. (A.3):

$$-\frac{1}{16} \left( \frac{du}{d\Phi} \right)^2 + \frac{1}{4} \frac{u}{\Phi} \frac{du}{d\Phi} - k_x u + A\Phi^2 + B\Phi^4 = 0. \quad (\text{A.5})$$

Rearrange Eq. (A.5) into a quadratic equation for  $du/d\Phi$  by multiplying through by  $-16$ :

$$\left( \frac{du}{d\Phi} \right)^2 - \left( 4 \frac{u}{\Phi} \right) \frac{du}{d\Phi} + (16k_x u - 16A\Phi^2 - 16B\Phi^4) = 0. \quad (\text{A.6})$$

## Step 2: Solve the First-Order ODE

Solve Eq. (A.6) for  $du/d\Phi$  using the quadratic formula. The discriminant is:

$$\Delta_{\text{quad}} = 16 \frac{u^2}{\Phi^2} - 64k_x u + 64A\Phi^2 + 64B\Phi^4. \quad (\text{A.7})$$

Taking the positive root (consistent with bounded physical solutions):

$$\frac{du}{d\Phi} = 2 \frac{u}{\Phi} + 2 \sqrt{\frac{u^2}{\Phi^2} - 4k_x u + 4A\Phi^2 + 4B\Phi^4}. \quad (\text{A.8})$$

Introduce a second substitution:  $\Psi = \Phi^2$  (i.e.,  $\Phi = \sqrt{\Psi}$  and  $d\Phi = d\Psi/(2\sqrt{\Psi})$ ). Since  $u = (\Phi')^2$ , rewrite  $u$  in terms of  $\Psi$  using the chain rule:

$$u = \left( \frac{d\Phi}{dy} \right)^2 = \left( \frac{d\Phi}{d\Psi} \frac{d\Psi}{dy} \right)^2 = \left( \frac{1}{2\sqrt{\Psi}} \frac{d\Psi}{dy} \right)^2 = \frac{1}{4\Psi} \left( \frac{d\Psi}{dy} \right)^2. \quad (\text{A.9})$$

Thus,  $\frac{d\Psi}{dy} = \pm 2\sqrt{\Psi}u$ . Substitute Eq. (A.9) and  $\Phi = \sqrt{\Psi}$  into Eq. (A.8). After simplifying the nested radicals and using  $\frac{du}{d\Phi} = 2\sqrt{\Psi} \frac{du}{d\Psi}$ , the equation reduces to:

$$\left( \frac{d\Psi}{dy} \right)^2 = 4B\Psi^3 + 4A\Psi^2 - 4k_x\Psi. \quad (\text{A.10})$$

## Step 3: Elliptic Integral to Jacobian Elliptic Cosine Function

Equation (A.10) is the canonical form of an elliptic integral. Assume the cubic polynomial  $P(\Psi) = 4B\Psi^3 + 4A\Psi^2 - 4k_x\Psi$  has three real roots ordered as  $\Psi_1 < \Psi_2 < \Psi_3$  with  $\Psi_2 \geq 0$  (ensuring  $\Psi = \Phi^2 \geq 0$  for physical solutions). Factor  $P(\Psi)$  into the standard form:

$$P(\Psi) = 4B(\Psi_3 - \Psi)(\Psi - \Psi_2)(\Psi - \Psi_1). \quad (\text{A.11})$$

Separate variables and integrate both sides of Eq. (A.10):

$$\int_{\Psi_2}^{\Psi} \frac{d\Psi}{\sqrt{4B(\Psi_3 - \Psi)(\Psi - \Psi_2)(\Psi - \Psi_1)}} = \pm y + C_0, \quad (\text{A.12})$$

where  $C_0$  is the constant of integration. Introduce the substitution  $z^2 = \frac{\Psi - \Psi_2}{\Psi_3 - \Psi_2}$ , so that:

$$\Psi = \Psi_2 + (\Psi_3 - \Psi_2)z^2, \quad (\text{A.13})$$

$$d\Psi = 2(\Psi_3 - \Psi_2)zdz. \quad (\text{A.14})$$

Substituting into Eq. (A.12) and absorbing constants into  $C_0$  and selecting the positive sign for physical consistency yields:

$$\int_0^z \frac{dz}{\sqrt{(1 - z^2)[1 - mz^2]}} = \sqrt{B(\Psi_3 - \Psi_1)} y + C_1, \quad (\text{A.15})$$

define the modular parameter  $m$ , which satisfies  $0 < m < 1$  for elliptic cosine solutions, as:

$$m = \frac{\Psi_3 - \Psi_2}{\Psi_3 - \Psi_1}. \quad (\text{A.16})$$

The integral is the standard Legendre form of the first-kind elliptic integral, whose inverse is the Jacobian elliptic cosine function  $\text{cn}(z, m)$ . Thus:

$$z = \text{cn} \left( \sqrt{B(\Psi_3 - \Psi_1)} y + C_1, m \right). \quad (\text{A.17})$$

For even solutions symmetric about  $y = 0$  (maximum at  $y = 0$ ), set  $C_1 = 0$ . Recalling  $\Psi = \Phi^2 = \Psi_2 + (\Psi_3 - \Psi_2)z^2$ , the physically bounded cnoidal wave solution is:

$$\Phi(y) = \sqrt{\Psi_2 + (\Psi_3 - \Psi_2) \cdot \text{cn}^2(\tilde{\alpha}y, m)}, \quad (\text{A.18})$$

where  $\tilde{\alpha} = \sqrt{B(\Psi_3 - \Psi_1)}$ . This solution oscillates between  $\sqrt{\Psi_2}$  (minimum) and  $\sqrt{\Psi_3}$  (maximum), consistent with  $\Psi = \Phi^2 \geq 0$ .

## Step 4: Parameter Constraints via Vieta's Formulas

The roots  $\Psi_1, \Psi_2, \Psi_3$  of the cubic polynomial  $P(\Psi) = 4B\Psi^3 + 4A\Psi^2 - 4k_x\Psi$  satisfy Vieta's formulas:

$$\Psi_1 + \Psi_2 + \Psi_3 = -\frac{A}{B}, \quad (\text{A.19})$$

$$\Psi_1\Psi_2 + \Psi_1\Psi_3 + \Psi_2\Psi_3 = -\frac{k_x}{B}, \quad (\text{A.20})$$

$$\Psi_1\Psi_2\Psi_3 = 0. \quad (\text{A.21})$$

These formulas relate the polynomial roots to the physical parameters  $k_x, A, B$ , with the normalization condition  $\int_{-\infty}^{\infty} \Phi^2(y)dy = 1$  used to fix remaining free parameters.

## Step 5: Special Limit – Bright Soliton ( $m \rightarrow 1$ )

As  $m \rightarrow 1$ ,  $\Psi_2 \rightarrow \Psi_3$ , and the Jacobian elliptic functions degenerate to hyperbolic functions (preserving physical boundedness):

$$\text{cn}(z, 1) = \text{sech}(z), \quad \text{sn}(z, 1) = \tanh(z).$$

The cnoidal wave solution reduces to the bright soliton form:

$$\Phi(y) = \sqrt{\Psi_2 + (\Psi_3 - \Psi_2) \cdot \text{sech}^2(\tilde{\alpha}y)}.$$

For zero-background bright solitons ( $\Psi_2 = 0$ , corresponding to  $\Phi \rightarrow 0$  as  $|y| \rightarrow \infty$ ), Eq. (A.21) is naturally satisfied, and the solution simplifies to:

$$\Phi_{\text{sol}}(y) = \sqrt{\Psi_3} \cdot \text{sech}(\tilde{\alpha}y), \quad (\text{A.22})$$

where  $\tilde{\alpha} = \sqrt{B(\Psi_3 - \Psi_1)}$ . For  $\Psi_1 = 0$ ,  $\tilde{\alpha} = \sqrt{B\Psi_3}$ .

## Step 6: Normalised Bright Soliton

Impose the normalization condition  $\int_{-\infty}^{\infty} \Phi^2(y)dy = 1$  on Eq. (A.22) (with  $\Psi_1 = 0$ ):

$$\int_{-\infty}^{\infty} \Psi_3 \text{sech}^2(\tilde{\alpha}y)dy = \frac{2\Psi_3}{\tilde{\alpha}} = 1.$$

Solve for  $\Psi_3$ :  $\Psi_3 = \tilde{\alpha}/2$ . Substitute into  $\tilde{\alpha} = \sqrt{B\Psi_3}$ :

$$\tilde{\alpha} = \sqrt{B \cdot \frac{\tilde{\alpha}}{2}} \implies \tilde{\alpha} = \frac{B}{2}.$$

Thus,  $\Psi_3 = B/4$ , and the normalized bright soliton solution is:

$$\Phi(y) = \frac{\sqrt{B}}{2} \operatorname{sech}\left(\frac{B}{2}y\right), \quad (\text{A.23})$$

which satisfies both the original CHJ equation and the normalisation condition.

## Step 7: Alternative Solution via Weierstrass $\wp$ -Function

As a complementary approach to the Jacobian elliptic function method presented in Steps 3–5, Eq. (A.10) admits an equivalent formulation in terms of the Weierstrass  $\wp$ -function. This representation is particularly advantageous for analyzing the complex structure of the solution manifold and provides a direct connection to the algebraic geometry of elliptic curves.

Starting from the canonical elliptic equation (A.10) with  $\Psi_1 = 0$ :

$$\left(\frac{d\Psi}{dy}\right)^2 = 4B\Psi(\Psi - \Psi_2)(\Psi - \Psi_3), \quad (\text{A.24})$$

we perform a linear transformation to eliminate the quadratic term, casting the cubic into the Weierstrass normal form. Let

$$\Psi(y) = \frac{1}{B} \left[ \zeta(y) - \frac{A}{3} \right], \quad (\text{A.25})$$

where  $A = -B(\Psi_2 + \Psi_3)$  follows from Vieta's formula (A.19). Substituting Eq. (A.25) into Eq. (A.24) and utilizing the identity  $4B\Psi^3 + 4A\Psi^2 - 4k_x\Psi = 4B\Psi(\Psi - \Psi_2)(\Psi - \Psi_3)$ , we obtain the standard Weierstrass differential equation:

$$\left(\frac{d\zeta}{dy}\right)^2 = 4\zeta^3 - g_2\zeta - g_3, \quad (\text{A.26})$$

with the invariants  $g_2$  and  $g_3$  given by

$$g_2 = \frac{4}{3}(A^2 + 3Bk_x), \quad (\text{A.27})$$

$$g_3 = \frac{4}{27}(-2A^3 - 9ABk_x). \quad (\text{A.28})$$

The roots  $e_1, e_2, e_3$  of the cubic polynomial  $4\zeta^3 - g_2\zeta - g_3$  are related to the physical parameters via

$$e_1 = B\Psi_3 + \frac{A}{3}, \quad e_2 = B\Psi_2 + \frac{A}{3}, \quad e_3 = \frac{A}{3}, \quad (\text{A.29})$$

satisfying  $e_1 + e_2 + e_3 = 0$  and  $e_1 > e_2 > e_3$  for  $B > 0$  and  $\Psi_3 > \Psi_2 > 0$ .

The general solution to Eq. (A.26) is expressed in terms of the Weierstrass  $\wp$ -function with invariants  $g_2, g_3$ :

$$\zeta(y) = \wp\left(\sqrt{B}y + C_0; g_2, g_3\right), \quad (\text{A.30})$$

where  $C_0$  is the integration constant determined by the initial condition  $\Psi(0) = \Psi_3$  (maximum amplitude). Consequently, the real amplitude  $\Phi(y)$  assumes the form

$$\Phi(y) = \sqrt{\frac{1}{B} \left[ \wp\left(\sqrt{B}y + C_0; g_2, g_3\right) - \frac{A}{3} \right]}. \quad (\text{A.31})$$

The Weierstrass solution (A.31) and the Jacobian solution (A.18) represent the same physical trajectory on the elliptic curve, related by a modular transformation. To establish their equivalence explicitly, we employ the fundamental identity connecting  $\wp$  and the Jacobian elliptic cosine  $\text{cn}$  when the cubic has three real roots:

$$\wp(z; g_2, g_3) = e_3 + \frac{e_1 - e_3}{\text{sn}^2(z\sqrt{e_1 - e_3}, \tilde{m})}, \quad (\text{A.32})$$

where the complementary modulus  $\tilde{m}$  is defined as

$$\tilde{m} = \frac{e_2 - e_3}{e_1 - e_3} = \frac{\Psi_2}{\Psi_3}. \quad (\text{A.33})$$

Using the identity  $\text{sn}^2(u, \tilde{m}) + \text{cn}^2(u, \tilde{m}) = 1$  and the relation between  $\tilde{m}$  and the modulus  $m$  of Eq. (A.18) (where  $m = 1 - \tilde{m} = \frac{\Psi_3 - \Psi_2}{\Psi_3}$ ), we transform Eq. (A.32) into

$$\wp(z) - \frac{A}{3} = B \left[ \Psi_2 + (\Psi_3 - \Psi_2) \text{cn}^2\left(z\sqrt{B\Psi_3}, m\right) \right]. \quad (\text{A.34})$$

Substituting  $z = \sqrt{B}y$  into Eq. (A.34) and comparing with Eq. (A.31), we recover precisely the Jacobian solution (A.18) with  $\tilde{\alpha} = \sqrt{B(\Psi_3 - \Psi_1)} = \sqrt{B\Psi_3}$  (since  $\Psi_1 = 0$ ). This confirms that

$$\Phi_{\text{Jacobi}}(y) = \Phi_{\text{Weierstrass}}(y), \quad (\text{A.35})$$

under the parameter mapping given by Eqs. (A.29) and (A.33).

In the soliton limit  $m \rightarrow 1^-$  (corresponding to  $\Psi_2 \rightarrow 0$  and  $e_2 \rightarrow e_3$ ), the lattice of the  $\wp$ -function degenerates such that  $\wp(z) \rightarrow e_3 + (e_1 - e_3)\text{csch}^2(z\sqrt{e_1 - e_3})$ . Using  $\text{csch}^2(u) = \text{sech}^2(u)$  for imaginary arguments or directly taking the limit  $\tilde{m} \rightarrow 0$ , Eq. (A.31) reduces to the normalized bright soliton (A.23), thereby verifying the consistency of both approaches in the integrable and non-periodic regimes.

Thus, the Weierstrass formulation provides an intrinsic geometric characterization of the solution space, while the Jacobian representation offers a computationally convenient form for physical applications. The equivalence demonstrated above ensures that the contact-geometric framework developed in the main text is independent of the specific parametrization of elliptic functions.

## References

- [1] Hazime Mori and Yoshiki Kuramoto. *Chaotic Bifurcations and Critical Phenomena*, pages 217–240. Springer Berlin Heidelberg, Berlin, Heidelberg, 1998. ISBN 978-3-642-80376-5. doi: [10.1007/978-3-642-80376-5\\_12](https://doi.org/10.1007/978-3-642-80376-5_12). URL [https://doi.org/10.1007/978-3-642-80376-5\\_12](https://doi.org/10.1007/978-3-642-80376-5_12).
- [2] Orazio Descalzi, M. Facão, M.I. Carvalho, Carlos Cartes, and Helmut R. Brand. Dissipative pulses stabilized by nonlinear gradient terms: A review of their dynamics and their interaction. *Physica D: Nonlinear Phenomena*, 473:134520, 2025. ISSN 0167-2789. doi: <https://doi.org/10.1016/j.physd.2024.134520>. URL <https://www.sciencedirect.com/science/article/pii/S0167278924004706>.
- [3] M. C. Cross and P. C. Hohenberg. Pattern formation outside of equilibrium. *Rev. Mod. Phys.*, 65:851–1112, Jul 1993. doi: [10.1103/RevModPhys.65.851](https://doi.org/10.1103/RevModPhys.65.851). URL <https://link.aps.org/doi/10.1103/RevModPhys.65.851>.
- [4] Wolfgang Schöpf and Walter Zimmermann. Convection in binary fluids: Amplitude

- equations, codimension-2 bifurcation, and thermal fluctuations. *Phys. Rev. E*, 47:1739–1764, Mar 1993. doi: 10.1103/PhysRevE.47.1739. URL <https://link.aps.org/doi/10.1103/PhysRevE.47.1739>.
- [5] A H Khater, D K Callebaut, and A R Seadawy. General soliton solutions for nonlinear dispersive waves in convective type instabilities. *Physica Scripta*, 74(3):384, aug 2006. doi: 10.1088/0031-8949/74/3/015. URL <https://doi.org/10.1088/0031-8949/74/3/015>.
- [6] Boris A. Malomed. Optical solitons and vortices in fractional media: A mini-review of recent results. *PHOTONICS*, 8(9), SEP 2021. doi: 10.3390/photonics8090353.
- [7] Jeffrey C.Y. Teo and Taylor L. Hughes. Topological defects in symmetry-protected topological phases. *Annual Review of Condensed Matter Physics*, 8 (Volume 8, 2017):211–237, 2017. ISSN 1947-5462. doi: <https://doi.org/10.1146/annurev-conmatphys-031016-025154>. URL <https://www.annualreviews.org/content/journals/10.1146/annurev-conmatphys-031016-025154>.
- [8] Igor S. Aranson and Lorenz Kramer. The world of the complex ginzburg-landau equation. *Rev. Mod. Phys.*, 74:99–143, Feb 2002. doi: 10.1103/RevModPhys.74.99. URL <https://link.aps.org/doi/10.1103/RevModPhys.74.99>.
- [9] Emmanuel Kengne. Modulational instability and soliton propagation in an alternate right-handed and left-handed multi-coupled nonlinear dissipative transmission network. *Chaos, Solitons & Fractals*, 146:110866, 2021. ISSN 0960-0779. doi: <https://doi.org/10.1016/j.chaos.2021.110866>. URL <https://www.sciencedirect.com/science/article/pii/S0960077921002198>.
- [10] EN Tsoy, A Ankiewicz, and N Akhmediev. Dynamical models for dissipative localized waves of the complex ginzburg-landau equation. *PHYSICAL REVIEW E*, 73(3, 2), MAR 2006. ISSN 2470-0045. doi: 10.1103/PhysRevE.73.036621.

- [11] Maria Blum, Christian Döding, and Patrick Henning. Vortex-capturing multiscale spaces for the ginzburg–landau equation. *Multiscale Modeling & Simulation*, 23(1):339–373, 2025. doi: 10.1137/24M1664538. URL <https://doi.org/10.1137/24M1664538>.
- [12] Robert W. Richardson. Ginzburg-landau theory of anisotropic superfluid neutron-star matter. *Physical Review D*, 5:1883–1896, 1972. URL <https://api.semanticscholar.org/CorpusID:120735026>.
- [13] Emmanuel Kengne, Wu-Ming Liu, Lars Q. English, and Boris A. Malomed. Ginzburg–landau models of nonlinear electric transmission networks. *Physics Reports*, 982:1–124, 2022. ISSN 0370-1573. doi: <https://doi.org/10.1016/j.physrep.2022.07.004>. URL <https://www.sciencedirect.com/science/article/pii/S037015732200268X>. Ginzburg-Landau models of nonlinear electric transmission networks.
- [14] J. D. Scheel, M. R. Paul, M. C. Cross, and P. F. Fischer. Traveling waves in rotating rayleigh-bénard convection: Analysis of modes and mean flow. *Phys. Rev. E*, 68:066216, Dec 2003. doi: 10.1103/PhysRevE.68.066216. URL <https://link.aps.org/doi/10.1103/PhysRevE.68.066216>.
- [15] Emmanuel Yomba and Poonam Ramchandra Nair. New coupled optical solitons to birefringent fibers for complex ginzburg-landau equations with hamiltonian perturbations and kerr law nonlinearity. *MATHEMATICS*, 12(19), OCT 2024. doi: 10.3390/math12193073.
- [16] Sachin Kumar, Saurabh Kumar Sharma, Ravi Karwasra, Sandeep Malik, Taher A. Nofal, and Ahmed H. Arnous. Soliton structures, bifurcation patterns, and chaos in a nonlinear transmission line governed by the modified complex ginzburg–landau equation. *Chaos, Solitons & Fractals*, 200:117068, 2025. ISSN 0960-0779. doi: <https://doi.org/10.1016/j.chaos.2025.117068>. URL <https://www.sciencedirect.com/science/article/pii/S0960077925010811>.

- [17] R. B. Hoyle. Zigzag and Eckhaus instabilities in a quintic-order nonvariational ginzburg-landau equation. *Phys. Rev. E*, 58:7315–7318, Dec 1998. doi: 10.1103/PhysRevE.58.7315. URL <https://link.aps.org/doi/10.1103/PhysRevE.58.7315>.
- [18] Robert A. Van Gorder. Complex ginzburg–landau equation for time-varying anisotropic media. *Studies in Applied Mathematics*, 153(3):e12730, 2024. doi: <https://doi.org/10.1111/sapm.12730>. URL <https://onlinelibrary.wiley.com/doi/abs/10.1111/sapm.12730>.
- [19] N. N. Akhmediev, A. Ankiewicz, and J. M. Soto-Crespo. Multisoliton solutions of the complex ginzburg-landau equation. *Phys. Rev. Lett.*, 79:4047–4051, Nov 1997. doi: 10.1103/PhysRevLett.79.4047. URL <https://link.aps.org/doi/10.1103/PhysRevLett.79.4047>.
- [20] Hadi Rezazadeh. New solitons solutions of the complex ginzburg-landau equation with kerr law nonlinearity. *OPTIK*, 167:218–227, 2018. ISSN 0030-4026. doi: 10.1016/j.ijleo.2018.04.026.
- [21] N Akhmediev, JM Soto-Crespo, and G Town. Pulsating solitons, chaotic solitons, period doubling, and pulse coexistence in mode-locked lasers: Complex ginzburg-landau equation approach - art. no. 056602. *PHYSICAL REVIEW E*, 63(5, 2), MAY 2001. ISSN 2470-0045. doi: 10.1103/PhysRevE.63.056602.
- [22] N Akhmediev and VV Afanasjev. Novel arbitrary-amplitude soliton solutions of the cubic-quintic complex ginzburg-landau equation. *Phys Rev Lett*, 75(12):2320–2323, Sep 1995. ISSN 1079-7114 (Electronic); 0031-9007 (Linking). doi: 10.1103/PhysRevLett.75.2320.
- [23] R. Montagne, E. Hernández-García, and M. San Miguel. Numerical study of a lyapunov functional for the complex ginzburg-landau equation. *Physica D: Nonlinear Phenomena*, 96(1):47–65, 1996. ISSN 0167-2789. doi: [https://doi.org/10.1016/0167-2789\(96\)80005-0](https://doi.org/10.1016/https://doi.org/10.1016/0167-2789(96)80005-0).

- 0167-2789(96)00013-9. URL <https://www.sciencedirect.com/science/article/pii/0167278996000139>.
- [24] Stefan C. Mancas and S. Roy Choudhury. Traveling wavetrains in the complex cubic–quintic ginzburg–landau equation. *Chaos, Solitons & Fractals*, 28(3):834–843, 2006. ISSN 0960-0779. doi: <https://doi.org/10.1016/j.chaos.2005.08.080>. URL <https://www.sciencedirect.com/science/article/pii/S0960077905006351>.
- [25] R. Abraham and J.E. Marsden. *Foundations of Mechanics*. Benjamin/Cummings Publishing Co., Reading, MA, USA, 1978. ISBN 0-8053-0102-X.
- [26] V. I. Arnold. *Mathematical Methods of Classical Mechanics*. Graduate Texts in Mathematics. Springer New York, New York, 2 edition, 12 2010. doi: <https://doi.org/10.1007/978-1-4757-2063-1>.
- [27] V. I. Arnold. *Contact Geometry and Wave Propagation: Lectures Given at the University of Oxford under the Sponsorship of the International Mathematical Union*. L’Enseignement mathématique, Université de Genève, Genève, 1989. URL <https://iucat.iu.edu/iub/86833>.
- [28] Alessandro Bravetti, Hans Cruz, and Diego Tapias. Contact Hamiltonian Mechanics. *Annals of Physics*, 376:17–39, 1 2017. ISSN 0003-4916. doi: <https://doi.org/10.1016/j.aop.2016.11.003>.
- [29] De Yu Zhong and Guang Qian Wang. Kinetic Equation for Stochastic Vector Bundles. *Journal of Physics A: Mathematical and Theoretical*, 57(22):225004, 5 2024. doi: <https://doi.org/10.1088/1751-8121/ad483a>.
- [30] Jordi Gaset, Xavier Gràcia, Miguel C. Muñoz Lecanda, Xavier Rivas, and Narsiso Román-Roy. New contributions to the hamiltonian and lagrangian contact formalisms for dissipative mechanical systems and their symmetries. *International Journal of Geometric Methods in Modern Physics*, 17(06):2050090, 2020. doi: 10.1142/S0219887820500905. URL <https://doi.org/10.1142/S0219887820500905>.

- [31] Kang-Jia Wang, Hong-Wei Zhu, Shuai Li, Feng Shi, Geng Li, and Xiao-Lian Liu. Bifurcation analysis, chaotic behaviors, variational principle, hamiltonian and diverse optical solitons of the fractional complex ginzburg-landau model. *INTERNATIONAL JOURNAL OF THEORETICAL PHYSICS*, 64(5), MAY 7 2025. ISSN 0020-7748. doi: 10.1007/s10773-025-05977-9.
- [32] Hansjörg Geiges. *An Introduction to Contact Topology*, volume 109 of *Cambridge Studies in Advanced Mathematics*. Cambridge University Press, London, 2008. doi: <https://doi.org/10.1017/CBO9780511611438>.
- [33] D.Y. Zhong and G.Q. Wang. Least constraint and contact dynamics of stochastic vector bundles. *Chaos, Solitons and Fractals*, 201:117143, 2025. ISSN 0960-0779. doi: <https://doi.org/10.1016/j.chaos.2025.117143>. URL <https://www.sciencedirect.com/science/article/pii/S0960077925011567>.
- [34] Alan C. Newell and J. A. Whitehead. Finite bandwidth, finite amplitude convection. *Journal of Fluid Mechanics*, 38(2):279–303, 1969. doi: 10.1017/S0022112069000176.
- [35] Lee A. Segel. Distant side-walls cause slow amplitude modulation of cellular convection. *Journal of Fluid Mechanics*, 38(1):203–224, 1969. doi: 10.1017/S0022112069000127.
- [36] Hongbo Jiang, Ruilong Song, Jiayi Shen, Zhiming Yang, Yuantong Liu, Xinxu Duan, Xiaoyun Tang, and Lei Jin. Transitions between periodic waves and soliton states in a polarization-dependent loss-tailored fiber laser. *Optics & Laser Technology*, 192: 113838, 2025. ISSN 0030-3992. doi: <https://doi.org/10.1016/j.optlastec.2025.113838>. URL <https://www.sciencedirect.com/science/article/pii/S003039922501429X>.
- [37] P.C. Hohenberg and A.P. Krekhov. An introduction to the ginzburg–landau theory of phase transitions and nonequilibrium patterns. *Physics Reports*, 572:1–42, 2015. ISSN 0370-1573. doi: <https://doi.org/10.1016/j.physrep.2015.01.001>. URL <https://www.sciencedirect.com/science/article/pii/S0370157315000514>.